Search for the α + core structure in the ground state bands of $22 \leqslant Z \leqslant 42$ even-even nuclei

M. A. Souza [*] and H. Miyake [†]
Instituto de Física, Universidade de São Paulo, Rua do Matão, 1371, CEP 05508-090, Cidade Universitária, São Paulo, São Paulo, Brazil

(Received 15 April 2021; accepted 15 November 2021; published 2 December 2021)

A systematic analysis of the α + core structure is performed in the ground state bands of even-even nuclei of the $22 \leqslant Z \leqslant 42$ region in terms of the local potential model. The α + core interaction is described by the nuclear potential of (1 + Gaussian)×(W.S. + W.S.^{3}) shape with two free parameters. Properties such as energy levels, reduced α widths, $B(E2)$ transition rates, and rms charge radii are calculated and compared with experimental data. A good agreement with the experimental data is obtained in general, even for the nuclei without the α + {doubly closed shell core} configuration. The analysis of the selected nuclei in the $22 \leqslant Z \leqslant 42$ region indicates that ^{44}Ti and ^{94}Mo have a greater α-clustering degree in comparison with their respective neighboring nuclei of this set. In addition, the model points to the existence of nuclei without the α + {doubly closed shell core} configuration with a significant α-clustering degree compared to ^{44}Ti, ^{60}Zn, and ^{94}Mo. The study shows that the α + core approach is satisfactorily applicable to nuclei other than those with α clustering above double-shell closures.

DOI: 10.1103/PhysRevC.104.064301

I. INTRODUCTION

Cluster models constitute a topic of nuclear physics in continuous development, being used for the investigation of properties in nuclei of different mass regions. The most recent challenges in the light mass region, such as the description of the Hoyle state, Hoyle-like states, and α gas states in general, are discussed by Schuck in Ref. [1], and the techniques applied in heavier nuclei, such as the antisymmetrized molecular dynamics, the quartetting wave function approach, etc. are detailed by Ren and Zhou in Ref. [2]. In the experimental field, an overview of the recent results in nuclear cluster physics is discussed in detail by Vardaci in Ref. [3].

An approach widely used in nuclear cluster physics is the local potential model (LPM), as presented originally by Buck, Dover, and Vary [4]. In this approach, the nucleus is assumed as a cluster + core system where the two components interact through a deep local potential $V(r)$ containing the nuclear and Coulomb terms; in the case where cluster and/or core has nonzero spin, terms resulting from noncentral forces are added, such as the spin-orbit term. In recent decades, α clustering has been analyzed by LPM in several studies emphasizing nuclei with the α + {doubly closed shell core} (hereafter α + DCSC) configuration, such as ^{20}Ne, ^{44}Ti, ^{52}Ti, ^{60}Zn, ^{94}Mo, and ^{212}Po (examples in Refs. [5–18]). In this way, some works demonstrate that nuclei with the α + DCSC configuration can be systematically analyzed with the same α + core potential type, providing a good general agreement with experimental data, as shown in Refs. [5,15,17–19]. In the recent work of Bai and Ren [19], a study of the α-cluster structure above double shell closures via double-folding potentials is shown, analyzing the ^{8}Be, ^{20}Ne, ^{44,52}Ti, and ^{212}Po nuclei; this study presents a detailed connection of the α + core potential with the chiral effective field theory.

Due to experimental data published in 2018 by Auranen *et al.* on ^{104}Te [20], further work was done on α clustering above the double shell closure at ^{100}Sn—such as that by Bai and Ren [21], Souza *et al.* [17], and Ibrahim *et al.* [18], and including the microscopic calculation of Yang *et al.* [22]—obtaining results compatible with the experimental α-decay half-life of ^{104}Te. Additional experimental data on energy levels, electromagnetic transition rates, half-lives of the excited states, etc. are needed to better evaluate the theoretical predictions on ^{104}Te.

In recent years, the Ti isotopes have been investigated theoretically and experimentally from the perspective of the α-cluster structure [16,23–25]. In the studies of Bailey *et al.* [23,24], a novel technique makes use of the continuous wavelet transform and machine learning to identify α-clustered states in ^{44,48,52}Ti through ^{4}He(^{40,44,48}Ca, α) resonant scattering measurements; such studies indicate the presence of the α + ^{40}Ca and α + ^{48}Ca structures in high-lying states of ^{44}Ti and ^{52}Ti, respectively. The results of Bailey *et al.* reinforce the indications of previous experiments which also point to the presence of the α-cluster structure in Ti isotopes, such as the ^{40,42,48}Ca(^{6}Li, d)^{44,46,52}Ti [26–30] and ^{40,42}Ca(^{7}Li, $t\alpha$)^{40,42}Ca [31] reactions and other α-transfer processes on Ca targets. The work of Ohkubo [16] discusses the α + ^{48}Ca structure in ^{52}Ti, using the optical potential model to analyze α + ^{48}Ca scattering data; the real part of the optical potential was used to calculate the α + ^{48}Ca energy bands, indicating that three ^{52}Ti experimental states found by Bailey *et al.* [23] are associated with the higher nodal positive parity band of the α + ^{48}Ca system.

About the Cr isotopic chain, the present authors investigated the α + core structure in ^{46}Cr and ^{54}Cr through

[*] marsouza@if.usp.br
[†] miyake@if.usp.br

LPM [32], introducing the use of the (1 + Gaussian)×(W.S. + W.S.^{3}) nuclear potential; the model showed good agreement with the energies of the ground state band and experimental $B(E2)$ transition rates, and it was shown that ^{46}Cr has a significant α-clustering degree compared to the well-studied ^{44}Ti. A similar study by Mohr [33] on ^{46}Cr and ^{54}Cr also showed satisfactory results for the same properties using a double-folding nuclear potential with the DDM3Y interaction. Previous works by Descouvemont [34] and Sakuda and Ohkubo [35] describe ^{48}Cr in terms of an $\alpha + \alpha + ^{40}$Ca system using the generator coordinate method and orthogonality condition model, respectively, obtaining good results in general for energy levels and $B(E2)$ rates.

A natural path in the development of the α-cluster model was its application in the $A \approx 90$ region, due to the proximity of the neutron shell closure at $N = 50$ and proton subshell closure at $Z = 40$. Calculations on ^{94}Mo in terms of an $\alpha + ^{90}$Zr system were made by different authors with favorable results [5,7,8,11,12,14,17,18]. In order to extend the application of the model to nuclei around ^{94}Mo, the present authors studied the α + core structure in ^{90}Sr, ^{92}Zr, ^{94}Mo, ^{96}Ru, and ^{98}Pd using the W.S. + W.S.^{3} nuclear potential [12], showing that LPM produces a good general description of the energy spectra, $B(E2)$ transition rates, and rms charge radii, suggesting a systematic behavior in their α + core structures. The previous work of Mohr [14] shows a similar treatment of the α + core system involving nuclei with $N = 52$ ($N_{\text{core}} = 50$) from ^{82}Zn to ^{104}Te, producing satisfactory results for the experimental $B(E2)$ rates without the use of effective charges; the double-folding nuclear potential used in Ref. [14] requires a strength parameter λ with a smooth dependence on the quantum number L to reproduce the experimental ground state bands.

Our studies in Refs. [12,17,32] suggest that LPM can be applied systematically in nuclei of distinct mass regions, including cases without the α + DCSC configuration. Therefore, the present work proposes a comprehensive study of the α + core structure in several even-even nuclei in the Z region delimited by two nuclei with a well-recognized α-cluster structure: ^{44}Ti and ^{94}Mo ($22 \leqslant Z \leqslant 42$ or $20 \leqslant Z_{\text{core}} \leqslant 40$). For this, the (1 + Gaussian)×(W.S. + W.S.^{3}) nuclear potential, with two free parameters and four fixed parameters, and already used successfully in Refs. [17,32], is applied in the present work. A comparative study of the nuclei selected in this region is carried out to identify those with higher degree of α clustering.

II. SELECTION OF NUCLEI FOR ANALYSIS

As exemplified in the previous section, a criterion applied commonly in studies on the α + core structure is the selection of nuclei with doubly or simply magic core. In the present study, we use the same criterion applied in our previous works [12,32] where the different even-Z isotopic chains are analyzed through the variation of binding energy per nucleon due to the α-core separation,

$$\frac{Q_\alpha}{A_T} = \frac{B_\alpha + B_{\text{core}} - B_T}{A_T}, \tag{1}$$

where Q_α is the Q value for α separation, A_T is the mass number of the total nucleus and B_α, B_{core}, and B_T are the experimental binding energies of the α cluster, core, and total nucleus, respectively. An absolute (or local) maximum of Q_α/A_T is considered to indicate the preferential nucleus for α clustering compared to the remaining (or neighboring) nuclei of the set. The values of B_α, B_{core}, and B_T are taken from Ref. [36].

There are nuclei in the $22 \leqslant Z \leqslant 42$ region with unmeasured spectra, especially unstable nuclei. Therefore, it is possible that the criterion described above selects nuclei in which there are insufficient experimental data for a consistent analysis of the α + core structure. Taking this possibility into account, a first additional condition is established for the selection of nuclei in the isotopic chain: (i) if the highest Q_α/A_T nucleus does not have at least some experimental energy levels with fairly defined spins and parities, one selects the isotope with the Q_α/A_T value immediately below which has more experimental energy levels with defined assignments. Also, a second condition is defined for an analysis of the influence of the shell closures on the α-clustering degree: (ii) the isotopes with doubly or simply magic core should be selected for a comparative study, provided they have at least some experimental energy levels with fairly defined spins and parities. The only exception to the selection criterion established is the inclusion of ^{48}Cr in the study, for the reason explained below.

Figure 1 shows graphically the Q_α/A_T values obtained for the even-even nuclei of the isotopic chains from Ti to Mo, indicating the nuclei selected for analysis. The selection of nuclei in each isotopic chain is detailed below:

Ti, Fe, Ni, and Zn: The ^{44}Ti, ^{58}Fe, ^{60}Ni, and ^{60}Zn nuclei are those with the highest Q_α/A_T values in their respective isotopic chains, and were selected for analysis. As the ^{52}Ti, ^{56}Fe, ^{58}Ni and ^{82}Zn nuclei have doubly or simply magic core, they were selected for a comparative study.

Cr: This isotopic chain was discussed in our previous work on ^{46,54}Cr [32]. ^{54}Cr has the highest Q_α/A_T value in the set of even-even isotopes (−146.8 keV). However, ^{46}Cr has a very close Q_α/A_T value (−147.7 keV) and has a magic $N_{\text{core}} = 20$. In this case, both were selected for analysis. As ^{48}Cr is pointed as a favorable nucleus for α clustering in Refs. [34,35], it was included in the comparative study exceptionally.

Ge, Se, Kr, and Sr: the nuclei ^{62}Ge, ^{64}Se, ^{70}Kr, and ^{74}Sr are those with the highest Q_α/A_T values in their respective isotopic chains. However, such nuclei have only the 0^+ ground state known experimentally, or the states above 0^+ have no defined spin and parity. For this reason, the neighboring isotopes with closest Q_α/A_T values and identified experimental levels were selected: ^{64}Ge, ^{68}Se, ^{72}Kr, and ^{78}Sr. The isotopes with magic $N_{\text{core}} = 50$ were also selected for a comparative study: ^{84}Ge, ^{86}Se, ^{88}Kr, and ^{90}Sr.

Zr: The three highest Q_α/A_T values in the set of even Zr isotopes are −31.825 keV, −32.072 keV, and −32.200 keV for ^{78}Zr, ^{80}Zr, and ^{92}Zr, respectively, according to the AME2016 binding energy data [36]. Such values

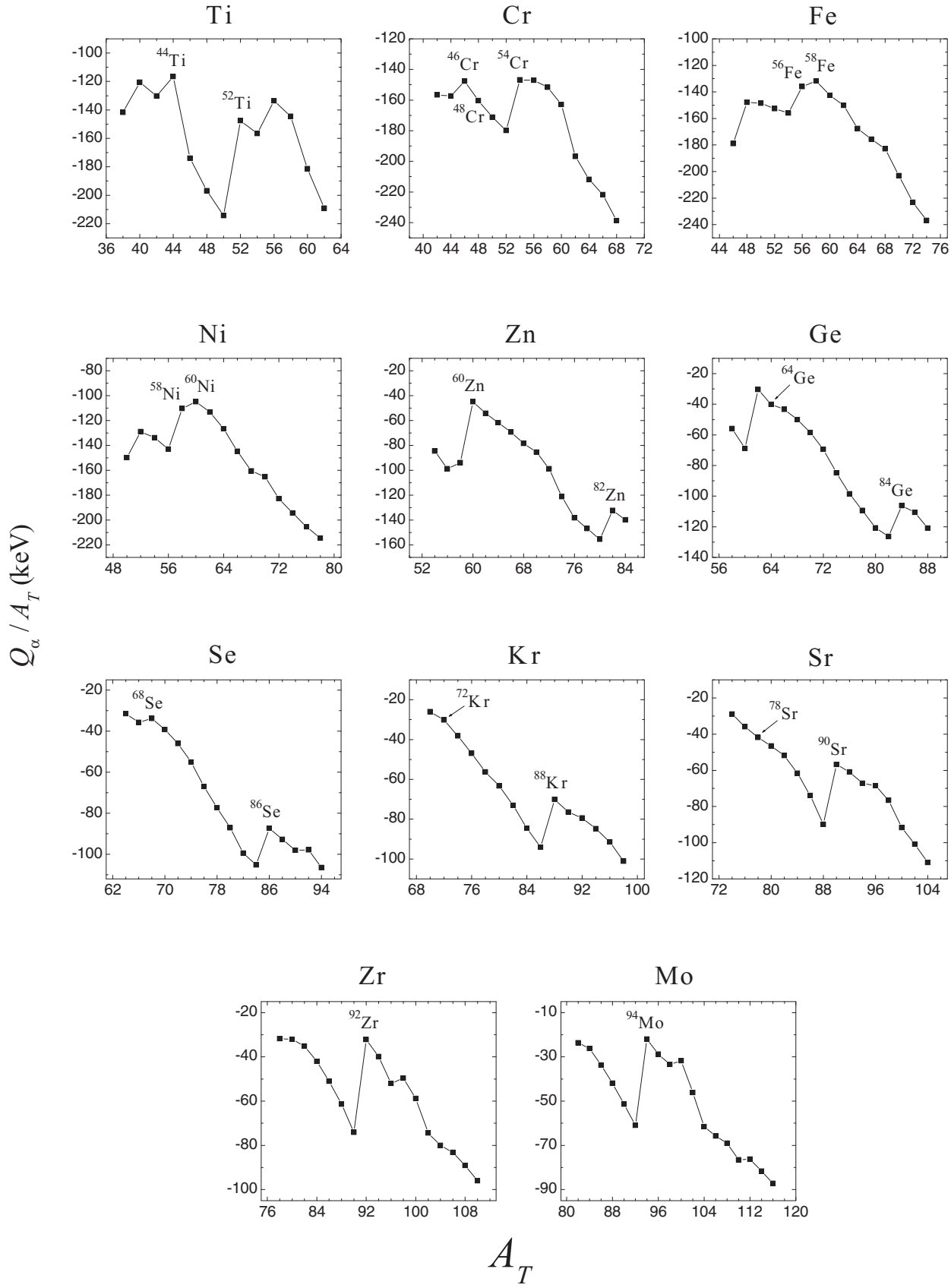

FIG. 1. Q_α/A_T values obtained for the α + core decomposition of even-even nuclei in the isotopic chains from Ti ($Z_T = 22$) to Mo ($Z_T = 42$) as a function of the total mass number A_T. The nuclei selected for the α-cluster analysis are indicated.

would lead to the selection of ^{78}Zr for analysis; however, using the binding energies from the AME2012 table [37], it is obtained that ^{92}Zr is the even isotope with highest Q_α/A_T. Due to the mentioned discordant results, and taking into account that ^{78}Zr and ^{80}Zr have only the 0^+ ground state with defined spin and parity, only ^{92}Zr was selected in this isotopic chain.

Mo: The ^{94}Mo nucleus is the one with the highest Q_α/A_T value in the set of even Mo isotopes. There are no other experimentally identified Mo isotopes with magic core. Therefore, only ^{94}Mo was selected.

Thus, a total of 21 even-even nuclei were selected for a systematic analysis of the α + core structure in the $22 \leqslant Z \leqslant 42$ region. The criterion defined by the absolute maximum Q_α/A_T value naturally selects the ^{44}Ti, ^{60}Zn, and ^{94}Mo nuclei with α + DCSC configuration, while the ^{52}Ti and ^{82}Zn nuclei, also with the α + DCSC configuration, were selected by condition *(ii)*.

The selected nuclei allow a broad study of the influence of the Q_α/A_T value and the magic core condition on the α-clustering degree, as seen in Sec. IV.

III. α-CLUSTER MODEL

The states of the total nucleus are described in terms of an α particle orbiting an inert core. The α + core interaction is described by the local potential

$$V(r) = V_N(r) + V_C(r) \tag{2}$$

with the nuclear and Coulomb terms. The Coulomb potential $V_C(r)$ is that of an α particle interacting with an uniformly charged spherical core of radius R. The intercluster nuclear potential $V_N(r)$ is given by the expression

$$V_N(r) = -V_0\left[1 + \lambda \exp\left(-\frac{r^2}{\sigma^2}\right)\right]\left\{\frac{b}{1+\exp[(r-R)/a]} + \frac{1-b}{\{1+\exp[(r-R)/3a]\}^3}\right\}, \tag{3}$$

where V_0, λ, a, and b are fixed parameters, and R and σ are variable parameters. The (1 + Gaussian)×(W.S. + W.S.^{3}) potential shape of Eq. (3) has already been successfully applied in our previous works on the α + core structure in ^{46,54}Cr [32], in the set {^{20}Ne, ^{44}Ti, ^{94}Mo, ^{212}Po} [17], and produced Q_α values and α-decay half-lives for ^{104}Te in agreement with experimental data [17] using the same fixed parameters.

The parameter values used are $V_0 = 220$ MeV, $a = 0.65$ fm, $b = 0.3$, and $\lambda = 0.14$, while R and σ are fitted specifically for each nucleus. Details on the origin of the parameter values, as well as the development of the (1 + Gaussian)× (W.S. + W.S.^{3}) shape, are explained in Refs. [17,32]. The variable parameters σ and R, shown in Table I, are fitted to provide the best possible reproduction of the 0^+ and 4^+ experimental levels of the ground state (g.s.) band.

The four nucleons of the α cluster must lie in shell-model orbitals outside those occupied by the core nucleons. This restriction is defined by the global quantum number $G = 2N + L$, where N is the number of internal nodes in the radial wave function and L is the orbital angular momentum. The quantum number $G_{\text{g.s.}}$ associated with the ground state band is shown in Table I for the selected nuclei. In accordance with the Wildermuth condition [38], $G_{\text{g.s.}} = 12$, 14, and 16 correspond to the $(pf)^4$, $(pf)^2(sdg)^2$, and $(sdg)^4$ configurations for the valence nucleons, respectively. The valence nucleons of ^{72}Kr and ^{78}Sr are in a transition region from the pf shell to the sdg shell; therefore, two numbers $G_{\text{g.s.}} = 12$ and 14 are tested to verify which is the most suitable in describing the g.s. bands of ^{72}Kr and ^{78}Sr, as discussed in more detail in Sec. IV.

TABLE I. Values of the parameters R and σ and the quantum number $G_{\text{g.s.}}$ for the nuclei studied.

Nucleus	$G_{\text{g.s.}}$	R (fm)	σ (fm)
^{44}Ti	12	4.551	0.425
^{52}Ti	12	4.612	0.382
^{46}Cr	12	4.658	0.248
^{48}Cr	12	4.684	0.215
^{54}Cr	12	4.674	0.210
^{56}Fe	12	4.694	0.303
^{58}Fe	12	4.690	0.307
^{58}Ni	12	4.680	0.510
^{60}Ni	12	4.670	0.545
^{60}Zn	12	4.611	0.320
^{82}Zn	14	5.367	0.204
^{64}Ge	12	4.647	0.278
^{84}Ge	14	5.339	0.236
^{68}Se	12	4.678	0.247
^{86}Se	14	5.326	0.289
^{72}Kr	12	4.724	0.000
	14	5.221	0.160
^{88}Kr	14	5.318	0.314
^{78}Sr	12	4.793	0.000
	14	5.294	0.000
^{90}Sr	14	5.321	0.318
^{92}Zr	14	5.295	0.248
^{94}Mo	16	5.783	0.410

The resolution of the Schrödinger radial equation for the α + core relative motion allows one to determine the energy levels of the system and respective radial wave functions, which are used to calculate other properties such as rms radii, electromagnetic transition rates, reduced α widths, etc.

IV. RESULTS

The calculated ground state bands are shown in Figs. 2–4 in comparison with experimental energies ([39], except [40] for ^{84}Ge). In general, the proposed α + core potential provides a satisfactory description of the experimental bands, mainly from 0^+ to 8^+. For the levels from 10^+ to 14^+, the calculated bands for ^{44,52}Ti, ^{46}Cr, ^{68}Se, ^{72}Kr (with $G_{\text{g.s.}} = 14$), and ^{92}Zr provide at least reasonable results. The (1 + Gaussian)×(W.S. + W.S.^{3}) potential generates a more compressed spacing at the highest spin levels, which differs more strongly from the corresponding experimental levels of some nuclei. However, most experimental levels above 8^+ have uncertain spin and/or parity, or have not been measured, which prevents a more accurate judgment of the high spin levels.

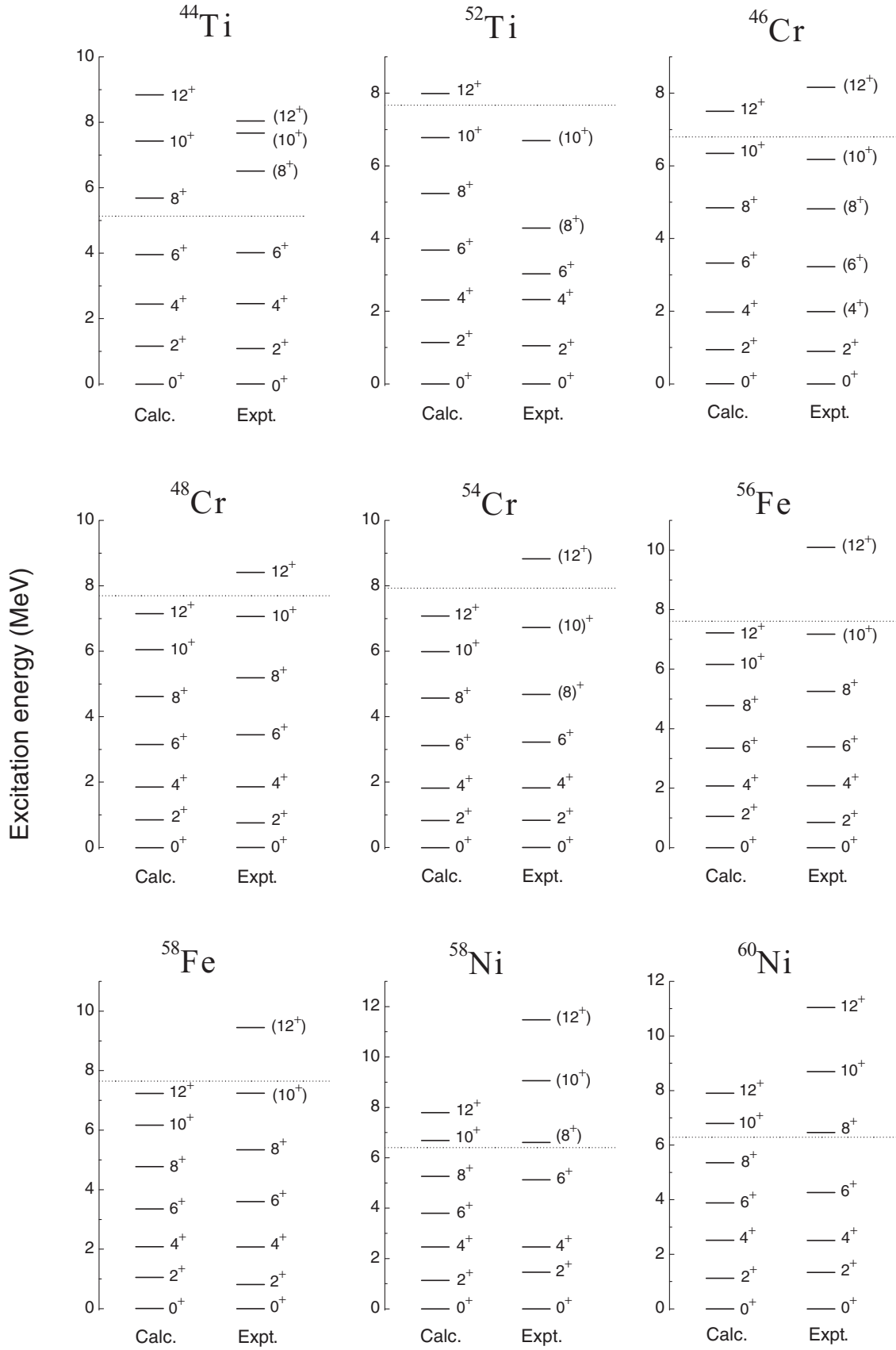

FIG. 2. Calculated energy levels for the ground state bands of the Ti, Cr, Fe, and Ni isotopes selected in this work in comparison with experimental energies. The dotted lines indicate the α + core thresholds.

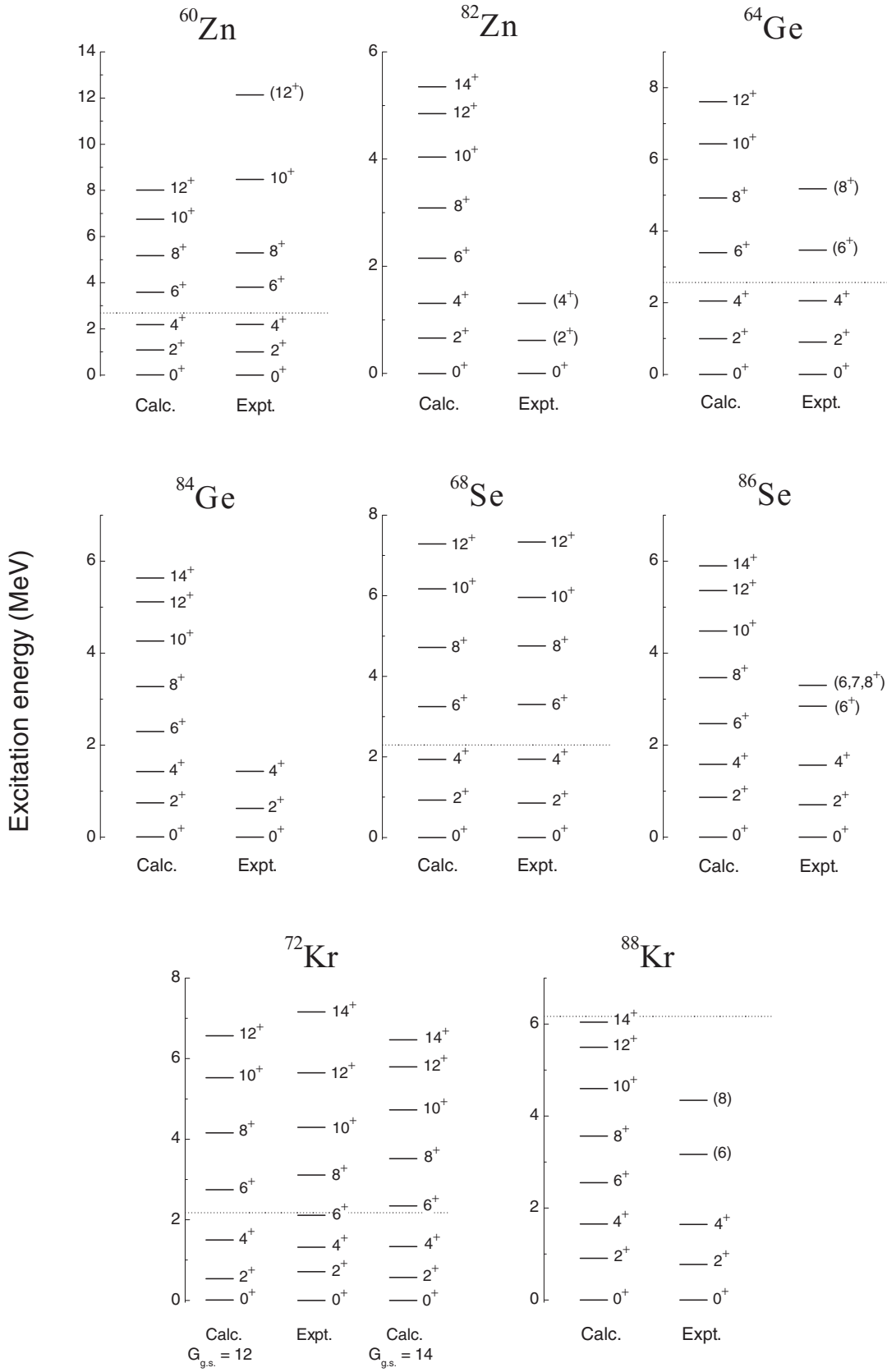

FIG. 3. Calculated energy levels for the ground state bands of the Zn, Ge, Se, and Kr isotopes selected in this work in comparison with experimental energies. The dotted lines indicate the α + core thresholds. In the cases of ^{82}Zn, ^{84}Ge, and ^{86}Se, the α + core thresholds are $E_{\text{thr.}} = 10.8493$, 8.9247, and 7.5130 MeV, respectively.

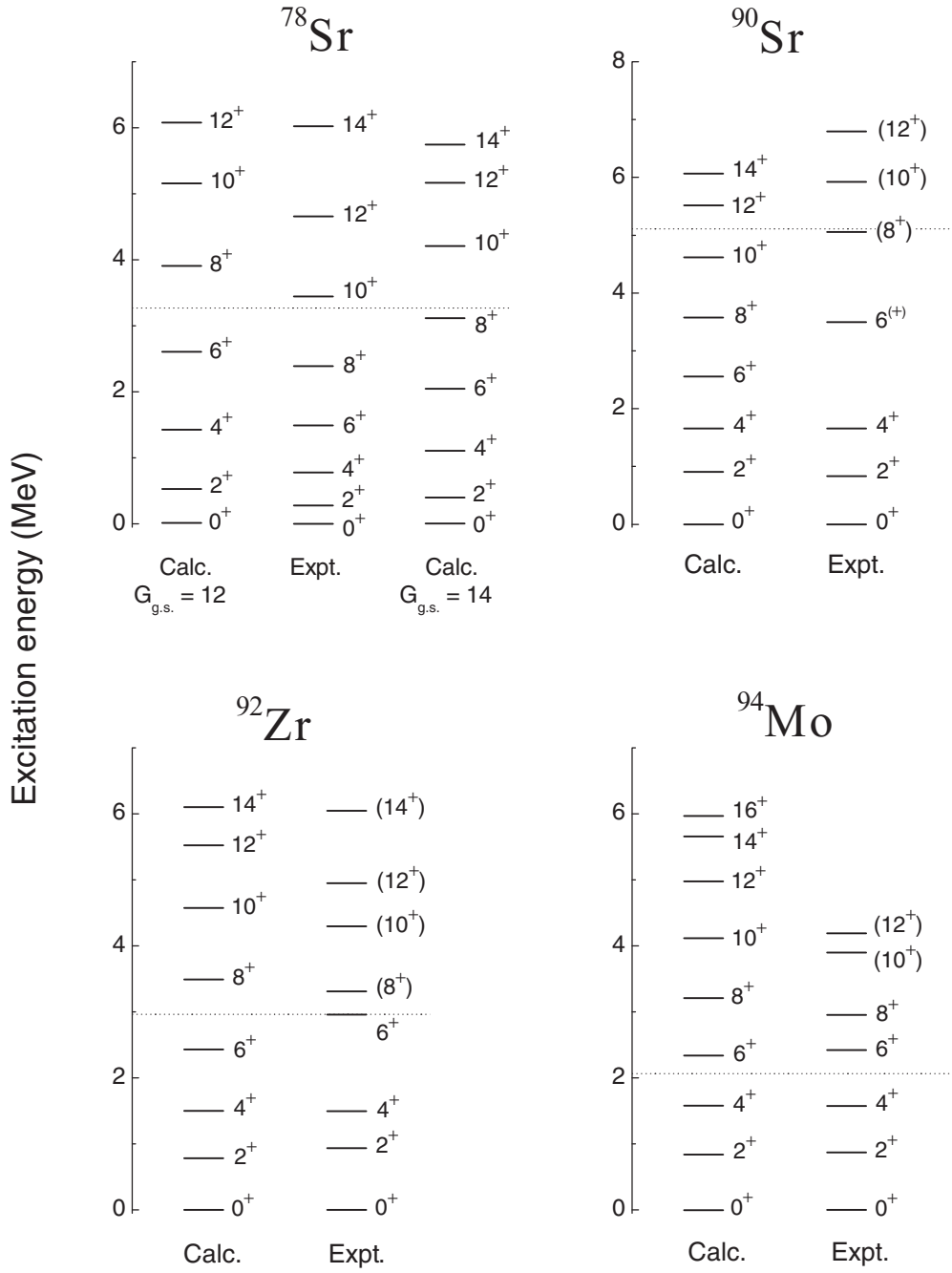

FIG. 4. Calculated energy levels for the ground state bands of the Sr, Zr, and Mo isotopes selected in this work in comparison with experimental energies. The dotted lines indicate the α + core thresholds.

For a better evaluation of the theoretical spectra, the standard deviation (S.D.) of the experimental energy levels in relation to the calculated energy levels is determined (see Table II), taking into account $n - p$ degrees of freedom, where n is the number of energy levels considered, and $p = 2$ is the number of free parameters of the α + core potential. Since most levels above 8^+ have uncertain spins and parities, or have not been measured, the calculation of S.D. considers only the levels from 0^+ to 8^+ for all nuclei ($n = 5$). Most of the calculated spectra have S.D. < 0.5 MeV, and the ^{46}Cr, ^{54}Cr, and ^{68}Se nuclei have S.D. < 100 keV, confirming the overall satisfactory result for the set of nuclei studied. An important feature is the existence of several nuclei with S.D. close to or smaller than those found for ^{44,52}Ti, ^{60}Zn, and ^{94}Mo. Therefore, the calculated g.s. bands show a good agreement with the experimental levels even for nuclei without the α + DCSC configuration.

The ^{72}Kr and ^{78}Sr nuclei have been analyzed in more detail with respect to the quantum number $G_{\text{g.s.}}$. As the mentioned nuclei have all experimental levels with defined spins and parities, it was possible to evaluate the most appropriate $G_{\text{g.s.}}$ number for describing their g.s. bands. In the case of

TABLE II. Standard deviations (S.D.) associated with the calculated g.s. bands of the nuclei studied, taking into account the levels from 0^+ to 8^+.

Nucleus	S.D. (MeV)
^{44}Ti	0.477
^{52}Ti	0.668
^{46}Cr	0.066
^{48}Cr	0.375
^{54}Cr	0.089
^{56}Fe	0.304
^{58}Fe	0.383
^{58}Ni	1.108
^{60}Ni	0.689
^{60}Zn	0.155
^{82}Zn	[a]
^{64}Ge	0.164
^{84}Ge	[a]
^{68}Se	0.057
^{86}Se	[a]
^{72}Kr ($G_{\text{g.s.}} = 12$)	0.721
^{72}Kr ($G_{\text{g.s.}} = 14$)	0.284
^{88}Kr	[a]
^{78}Sr ($G_{\text{g.s.}} = 12$)	1.159
^{78}Sr ($G_{\text{g.s.}} = 14$)	0.565
^{90}Sr	1.012
^{92}Zr	0.333
^{94}Mo	0.155

[a]Not calculated, as the experimental levels 6^+ and 8^+ are not measured or have undefined spin and parity.

$G_{\text{g.s.}} = 12$, it is noted that the experimental bands of ^{72}Kr and ^{78}Sr are very compressed compared to the calculated bands, while in the case of $G_{\text{g.s.}} = 14$, this difference is considerably reduced (see Figs. 3 and 4). This feature is also noted in Table II, where S.D.(^{72}Kr) is reduced from 0.721 to 0.284 MeV and S.D.(^{78}Sr) is reduced from 1.159 to 0.565 MeV when $G_{\text{g.s.}}$ is increased from 12 to 14. This is a first indication that the number $G_{\text{g.s.}} = 14$ is the most suitable for describing the ground state bands of ^{72}Kr and ^{78}Sr, which suggests the $(pf)^2(sdg)^2$ configuration for valence nucleons according to the Wildermuth condition.

Shell-model calculations indicate that ^{72}Kr has a prolate-oblate coexistence, as do other nuclei at or near the $N = Z$ line in the $70 \leqslant A \leqslant 80$ mass region [41]. It is known that the energy sequence of shell-model orbits can undergo strong changes in deformed nuclei, including allowing the $g_{9/2}$ orbit to approach the pf-shell orbitals and become an intruder orbit in this shell [42]. The ^{78}Sr nucleus has $Z = 38$ and $N = 40$, i.e., two closed subshells, meaning that the excitation of the two valence neutrons of the α-cluster must lead to the occupation of the $g_{9/2}$ orbit. Therefore, it is reasonable that the $(pf)^2(sdg)^2$ configuration is associated with the ^{72}Kr and ^{78}Sr yrast bands.

Consulting the nuclear data tables [39] and more recent publications [43], it is verified that 10 of the 21 nuclei analyzed have energy levels of the g.s. band populated in α-transfer reactions (see Table III); such experimental results can be interpreted as indications of the α-cluster structure

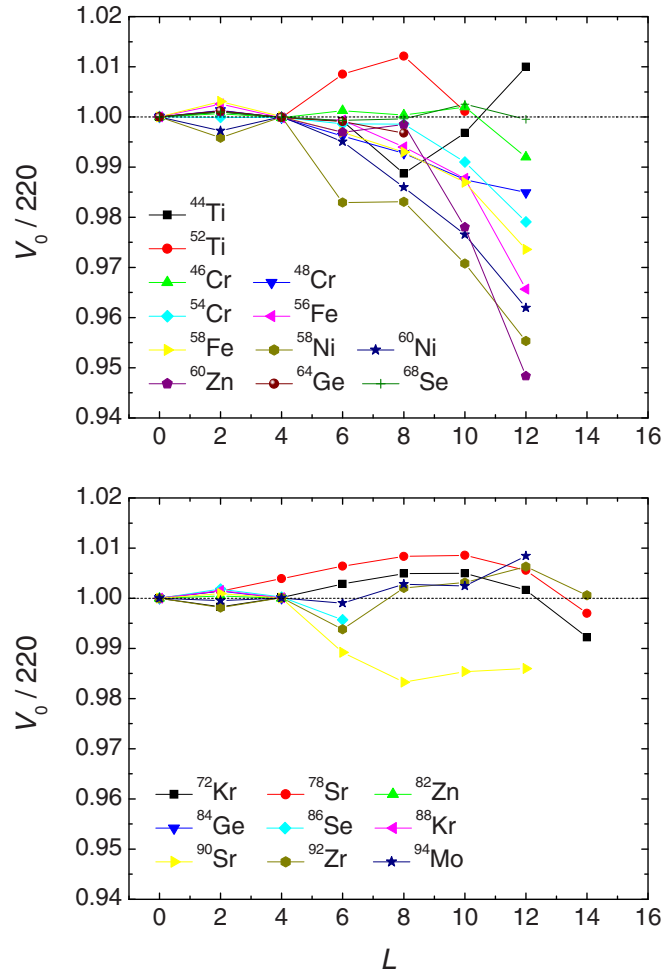

FIG. 5. Values of the ratio $V_0/220$ as a function of the quantum number L. The V_0 values have been fitted to precisely reproduce the experimental energy levels L^π of the g.s. bands. The dotted line corresponds to $V_0/220 = 1$. The values of $V_0/220$ shown for ^{72}Kr and ^{78}Sr correspond to $G_{\text{g.s.}} = 14$.

in these nuclei. The ^{44}Ti nucleus is the most studied by this mode, with several α-transfer processes, where all levels of the g.s. band have been identified. In other nuclei analyzed, the g.s. bands are identified by α-transfer reactions only partially, or there are no data referring to α transfer. The ^{90}Sr and ^{92}Zr nuclei have the levels from 0^+ to 12^+ of the g.s. band populated through the ^{12}C(^{86}Kr, $2\alpha\gamma$)^{90}Sr and ^{88}Sr(^{7}Li, $2np\gamma$)^{92}Zr reactions, respectively. In the case of the ^{90}Zr(^{6}Li, d)^{94}Mo reaction, the experimental results for the ^{94}Mo levels from 0^+ to 6^+ are not conclusive, due to the huge background peaks resulting from carbon and oxygen contaminants on the target, making it difficult to clearly identify the ^{94}Mo levels. However, the ^{94}Mo levels from 0^+ to 6^+ are identified through the ^{90}Zr(^{16}O, ^{12}C γ)^{94}Mo reaction.

The deviations between theoretical and experimental levels of the g.s. bands can be analyzed in terms of a dependence of the quantum number L. Figure 5 shows graphically the values of $V_0/220$ as a function of L, where the depth parameter V_0 has been fitted to precisely reproduce each experimental energy level. The calculation of $V_0/220$ allows analyzing the relative

TABLE III. Energy levels populated in α-transfer reactions in the ground state bands of the nuclei under study. Additionally, the energy levels populated in the ^{12}C(^{86}Kr, $2\alpha\gamma$)^{90}Sr pickup reaction (related to ^{90}Sr) are shown. At the first mention of each experimental level, its corresponding excitation energy is indicated in MeV. Experimental data from Ref. [39], except where indicated.

Nucleus	Reaction	Levels populated in the g.s. band
^{44}Ti	^{40}Ca(α, γ)	0^+ (g.s.), 2^+ (1.083), 4^+ (2.454), 6^+ (4.015)
	^{40}Ca(^{6}Li, d)	0^+, 2^+, 4^+, 6^+, (8^+) (6.508)
	^{40}Ca(pol ^{6}Li, d), (^{6}Li, $pn\gamma$)	0^+, 2^+, 4^+, 6^+
	^{40}Ca(^{7}Li, t)	0^+, 2^+
	^{40}Ca(^{12}C, ^{8}Be)	0^+, 2^+
	^{40}Ca(^{13}C, ^{9}Be), (^{14}N, ^{10}B)	0^+
	^{40}Ca(^{16}O, ^{12}C)	0^+, 4^+, 6^+, (8^+), (10^+) (7.671), (12^+) (8.040)
	^{40}Ca(^{20}Ne, ^{16}O)	0^+, 2^+, 4^+, 6^+
	^{40}Ca(^{32}S, ^{28}Si)	0^+
	^{40}Ca(^{6}Li, $pn\gamma$) [44]	0^+, 2^+, 4^+, 6^+, (8^+), (10^+), (12^+)
^{52}Ti	^{48}Ca(^{6}Li, d)	0^+ (g.s.), 2^+ (1.050)
	^{48}Ca(^{7}Li, $p2n\gamma$)	0^+, 2^+, 4^+ (2.318), 6^+ (3.029)
	^{48}Ca(^{12}C, ^{8}Be)	0^+, 2^+, 4^+
	^{48}Ca(^{16}O, ^{12}C)	0^+, 2^+
^{54}Cr	^{50}Ti(^{6}Li, d)	0^+ (g.s.), 2^+ (0.835), 4^+ (1.824)
	^{50}Ti(^{16}O, ^{12}C)	0^+, 2^+, 4^+
^{56}Fe	^{52}Cr(^{6}Li, d)	0^+ (g.s.), 2^+ (0.847), 4^+ (2.085)
^{58}Fe	^{54}Cr(^{6}Li, d)	0^+ (g.s.), 2^+ (0.811)
^{58}Ni	^{54}Fe(^{6}Li, d)	0^+ (g.s.), 2^+ (1.454), 4^+ (2.459), 6^+ (5.128)
	^{54}Fe(^{7}Li, t)	0^+, 2^+
	^{54}Fe(^{12}C, ^{8}Be)	0^+, 2^+, 4^+
	^{54}Fe(^{16}O, ^{12}C)	0^+, 2^+, 4^+
^{60}Ni	^{56}Fe(^{6}Li, d)	0^+ (g.s.), 2^+ (1.333), 4^+ (2.506)
	^{56}Fe(^{7}Li, $2np\gamma$)	0^+, 2^+, 4^+, 6^+ (4.265)
^{90}Sr	^{12}C(^{86}Kr, $2\alpha\gamma$)	0^+ (g.s.), 2^+ (0.832), 4^+ (1.656), $6^{(+)}$ (3.495), (8^+) (5.056), (10^+) (5.924), (12^+) (6.795)
^{92}Zr	^{88}Sr(^{7}Li, $2np\gamma$)	0^+ (g.s.), 2^+ (0.935), 4^+ (1.495), 6^+ (2.957), (8^+) (3.309), (10^+) (4.297), (12^+) (4.947)
^{94}Mo	^{90}Zr(^{16}O, ^{12}C γ)	0^+ (g.s.), 2^+ (0.871), 4^+ (1.574), 6^+ (2.423)
	^{90}Zr(^{6}Li, d) [29,30]	*not conclusive*: 0^+, 2^+, 4^+, 6^+

variation of V_0 compared to the fixed value of 220 MeV previously applied in the description of the g.s. bands. It is noted that the relative variation of V_0 is very small in general in the $0 \leqslant L \leqslant 8$ range: in most energy levels of this range, the relative variation of V_0 is between -1% and 1%. In the $10 \leqslant L \leqslant 14$ range, the variation of V_0 is a little greater, but still relatively small: the highest relative variations (in modulus) occur at $L = 12$ in the ^{56}Fe, ^{58}Ni, ^{60}Ni, and ^{60}Zn nuclei, between 3% and 5% approximately; such nuclei have experimental g.s. bands with an approximately rotational behavior, which differ more strongly from the calculated bands at the highest spin levels. Therefore, it is shown that the α + core potential used in this work is weakly L dependent. Such dependence can not be described solely by a fitted function $V_0(L)$, as there is not a similar behavior among the 21 nuclei analyzed.

Table IV shows the properties calculated for the selected nuclei in the 0^+ ground state: reduced α width (γ_α^2), dimensionless reduced α width (θ_α^2), rms intercluster separation ($\langle R^2\rangle^{1/2}$), the ratio of $\langle R^2\rangle^{1/2}$ to the sum of the experimental rms charge radii of α and core,

$$\mathcal{R} = \frac{\langle R^2\rangle^{1/2}}{\langle r^2\rangle_\alpha^{1/2} + \langle r^2\rangle_{\text{core}}^{1/2}}, \tag{4}$$

the rms charge radius predicted by the model for the total nucleus ($\langle r^2\rangle_T^{1/2}$), the ratio of $\langle r^2\rangle_T^{1/2}$ to the corresponding experimental value ($\langle r^2\rangle_T^{1/2}/\langle r^2\rangle_{T\,\text{exp}}^{1/2}$), and the ratios of γ_α^2 to the reduced α widths of the α + DCSC nuclei: ^{44}Ti, ^{60}Zn, and ^{94}Mo. The values of $\mathcal{R}$, $\langle r^2\rangle_T^{1/2}$, and $\langle r^2\rangle_T^{1/2}/\langle r^2\rangle_{T\,\text{exp}}^{1/2}$ were not calculated for some nuclei due to the lack of experimental rms radius data for the core or the total nucleus. For a better evaluation of the $G_{\text{g.s.}}$ number in ^{72}Kr, an estimate of the rms charge radius of the respective core (^{68}Se) is made through a proportion relation with $A^{1/3}$ and taking the experimental rms charge radius of ^{72}Kr as reference.

The reduced α width is defined as [46,47]

$$\gamma_\alpha^2 = \left(\frac{\hbar^2}{2\mu a_c}\right) u^2(a_c) \left[\int_0^{a_c} |u(r)|^2 dr\right]^{-1}, \tag{5}$$

where μ is the reduced mass of the system, $u(r)$ is the radial wave function of the state and a_c is the channel radius. The dimensionless reduced α width θ_α^2 is defined as the ratio of γ_α^2 to the Wigner limit,

$$\theta_\alpha^2 = \frac{2\mu a_c^2}{3\hbar^2}\gamma_\alpha^2. \tag{6}$$

TABLE IV. Calculated values for the reduced α width (γ_α^2), dimensionless reduced α width (θ_α^2), rms intercluster separation ($\langle R^2\rangle^{1/2}$), the ratio $\mathcal{R}$ [see Eq. (4)], rms charge radius predicted for the total nucleus ($\langle r^2\rangle_T^{1/2}$), the ratio of $\langle r^2\rangle_T^{1/2}$ to the corresponding experimental rms charge radius ($\langle r^2\rangle_{T\,\mathrm{exp}}^{1/2}$) [45], and the ratios of γ_α^2 to the reduced α widths of ^{44}Ti, ^{60}Zn, and ^{94}Mo, referring to the 0^+ ground state of the nuclei studied. The channel radius used for the calculation of γ_α^2 and θ_α^2 is obtained from Eq. (7) (see details in the text).

Nucleus	γ_α^2 (keV)	θ_α^2 (10^{-3})	$\langle R^2\rangle^{1/2}$ (fm)	$\mathcal{R}$	$\langle r^2\rangle_T^{1/2}$ (fm)	$\langle r^2\rangle_T^{1/2}/\langle r^2\rangle_{T\,\mathrm{exp}}^{1/2}$	γ_α^2 / $\gamma_\alpha^2(^{44}\mathrm{Ti})$	γ_α^2 / $\gamma_\alpha^2(^{60}\mathrm{Zn})$	γ_α^2 / $\gamma_\alpha^2(^{94}\mathrm{Mo})$
^{44}Ti	3.644	11.453	4.412	0.8562	3.5858	0.9929	1.000	6.166	4.364
^{52}Ti	1.936	6.178	4.310	0.8365	3.5756		0.531	3.276	2.319
^{46}Cr	1.855	5.968	4.339				0.509	3.139	2.222
^{48}Cr	0.924	3.107	4.311	0.8154	3.6891		0.254	1.563	1.107
^{54}Cr	1.013	3.375	4.290	0.8178	3.6506	0.9897	0.278	1.714	1.213
^{56}Fe	0.600	2.071	4.276	0.8037	3.7122	0.9932	0.165	1.015	0.719
^{58}Fe	0.456	1.606	4.271	0.7962	3.7511	0.9938	0.125	0.772	0.546
^{58}Ni	0.479	1.693	4.280	0.7972	3.7526	0.9939	0.131	0.810	0.574
^{60}Ni	0.375	1.353	4.278	0.7903	3.7931	0.9951	0.103	0.635	0.449
^{60}Zn	0.591	2.185	4.370				0.162	1.000	0.708
^{82}Zn	0.208	0.850	4.587				0.057	0.352	0.249
^{64}Ge	0.333	1.277	4.350				0.091	0.563	0.399
^{84}Ge	0.232	0.953	4.607	0.8083	4.0748		0.064	0.393	0.278
^{68}Se	0.194	0.770	4.335				0.053	0.328	0.232
^{86}Se	0.158	0.674	4.621				0.043	0.267	0.189
^{72}Kr ($G_{\mathrm{g.s.}} = 12$)	0.119	0.489	4.328	0.7513[a]	4.1108[a]	0.9874	0.033	0.201	0.143
^{72}Kr ($G_{\mathrm{g.s.}} = 14$)	0.771	3.163	4.760	0.8263[a]	4.1358[a]	0.9933	0.212	1.305	0.923
^{88}Kr	0.132	0.575	4.636				0.036	0.223	0.158
^{78}Sr ($G_{\mathrm{g.s.}} = 12$)	0.031	0.137	4.282	0.7304	4.2036	0.9877	0.009	0.052	0.037
^{78}Sr ($G_{\mathrm{g.s.}} = 14$)	0.233	1.016	4.712	0.8038	4.2265	0.9930	0.064	0.394	0.279
^{90}Sr	0.135	0.591	4.646	0.7930	4.2197	0.9903	0.037	0.228	0.162
^{92}Zr	0.154	0.687	4.682	0.7936	4.2582	0.9890	0.042	0.261	0.184
^{94}Mo	0.835	3.792	5.104	0.8586	4.3215	0.9928	0.229	1.413	1.000

[a]For the calculation of the indicated values, an estimate of the rms charge radius of the core is made through a proportion relation with $A^{1/3}$ and taking as reference the experimental rms charge radius of ^{72}Kr.

The calculation of γ_α^2 and θ_α^2 depends on the choice of the channel radius a_c for each nucleus. In our previous works [12,17,32], a_c was determined through a linear relation with $A_\alpha^{1/3} + A_{\mathrm{core}}^{1/3}$. As the present work compares isotopes with very close mass numbers, it is convenient that the channel radius varies as a function of the nuclear radius more precisely. Thus, a_c is given by the equation

$$a_c = 1.8514 + 1.5853\,\langle r^2\rangle_{\mathrm{core}}^{1/2}\ (\mathrm{fm}). \tag{7}$$

The parameters of Eq. (7) were fitted to minimize possible discrepancies with the a_c values predicted for ^{20}Ne, ^{44}Ti, ^{94}Mo, and ^{212}Po by the formula used in Refs. [12,17,32]. For the cores where $\langle r^2\rangle_{\mathrm{core}}^{1/2}$ is known experimentally, a_c is determined by using the tabulated values from Refs. [45,48], and for the nuclei where $\langle r^2\rangle_{\mathrm{core}}^{1/2}$ is unmeasured, the formula [49]

$$\langle r^2\rangle^{1/2} = 0.966\left(1 - 0.182\frac{N-Z}{A} + \frac{1.652}{A}\right)A^{1/3}\ (\mathrm{fm}) \tag{8}$$

is applied, which describes with good accuracy the tabulated experimental rms charge radii from Ref. [45].

Analyzing the selected nuclei, it is noted that the values of $\gamma_\alpha^2(0^+)$ and $\theta_\alpha^2(0^+)$ for ^{44}Ti and ^{94}Mo are considerably higher than the values obtained for other nuclei in their respective mass subregions (see the ratios γ_α^2 / $\gamma_\alpha^2(^{44}\mathrm{Ti})$ and γ_α^2 / $\gamma_\alpha^2(^{94}\mathrm{Mo})$ in Table IV), corroborating the statement that ^{44}Ti and ^{94}Mo are preferential nuclei for α clustering. This statement is reinforced by the ratio $\mathcal{R}$, since $\mathcal{R}(^{44}\mathrm{Ti})$ is considerably higher than the $\mathcal{R}$ values for the selected nuclei from ^{46}Cr to ^{60}Ni, and $\mathcal{R}(^{94}\mathrm{Mo})$ is considerably higher than the $\mathcal{R}$ values for the selected nuclei from ^{78}Sr to ^{92}Zr. The ^{60}Zn nucleus has values of $\gamma_\alpha^2(0^+)$ and $\theta_\alpha^2(0^+)$ reasonably higher than in neighboring nuclei of the set [see the ratio γ_α^2 / $\gamma_\alpha^2(^{60}\mathrm{Zn})$], indicating that its α + DCSC condition also favors it for α clustering in its subregion.

It should be taken into account that $G_{\mathrm{g.s.}} = 16$ for ^{94}Mo, while other nuclei selected in the same mass subregion have $G_{\mathrm{g.s.}} = 14$, which implies lower values of the parameter R for the nuclei with smaller $G_{\mathrm{g.s.}}$ and, consequently, smaller reduced α widths and rms separations. However, Ref. [12] indicates that ^{96}Ru and ^{98}Pd, which are neighbors of ^{94}Mo and have $G_{\mathrm{g.s.}} = 16$, present $\gamma_\alpha^2(0^+)$ and $\langle R^2\rangle^{1/2}(0^+)$ values smaller than in ^{94}Mo, corroborating the statement that ^{94}Mo is a preferential nucleus for α clustering in its subregion. In addition, it should be mentioned that our recent calculation [17] suggest that ^{104}Te has an α + core structure even more pronounced than in ^{94}Mo, with $\gamma_\alpha^2(0^+) \approx 1$ keV.

The γ_α^2 / $\gamma_\alpha^2(^{44}\mathrm{Ti})$, γ_α^2 / $\gamma_\alpha^2(^{60}\mathrm{Zn})$, and γ_α^2 / $\gamma_\alpha^2(^{94}\mathrm{Mo})$ ratios are shown in Table IV for a comparison of the α-clustering degree in the ground states of the selected nuclei in relation to ^{44}Ti, ^{60}Zn, and ^{94}Mo. The α + DCSC nuclei ^{52}Ti and ^{82}Zn

were not included as reference elements in the systematic comparison, since they have relatively lower reduced α widths within their mass subregions. It is convenient that the comparison of reduced α widths is done mainly between nuclei of the same mass subregion, as there is a trend to reduce the average magnitude of γ_α^2 from a region of lighter mass to a region of heavier mass. In this way, it is seen there are nuclei with a considerable α-clustering degree compared to ^{44}Ti in its subregion, with the following $\gamma_\alpha^2/\gamma_\alpha^2(^{44}\text{Ti})$ ratios: ^{52}Ti (0.531), ^{46}Cr (0.509), ^{54}Cr (0.278), and ^{48}Cr (0.254). The ^{48}Cr nucleus, which was included in the comparative study exceptionally (see Sec. II), has the smallest $\gamma_\alpha^2/\gamma_\alpha^2(^{44}\text{Ti})$ value among the ^{46,48,54}Cr isotopes, but it is indicated that ^{48}Cr and ^{54}Cr have a similar α-clustering degree from the viewpoint of the α + core structure.

Compared to ^{60}Zn, there are nuclei with a significant α-clustering degree in its subregion, with the following $\gamma_\alpha^2/\gamma_\alpha^2(^{60}\text{Zn})$ ratios: ^{56}Fe (1.015), ^{58}Fe (0.772), ^{58}Ni (0.810), ^{60}Ni (0.635), ^{64}Ge (0.563), and ^{68}Se (0.328); i.e., there are nuclei without the α + DCSC configuration with a similar or considerable α-clustering degree compared to ^{60}Zn.

In the ^{94}Mo subregion, the analyzed nuclei (^{82}Zn, ^{84}Ge, ^{86}Se, ^{88}Kr, ^{90}Sr, and ^{92}Zr) have $\gamma_\alpha^2/\gamma_\alpha^2(^{94}\text{Mo}) < 0.3$, showing a more relevant α-clustering degree for ^{82}Zn (0.249) and ^{84}Ge (0.278). Although this work focuses on the $22 \leqslant Z \leqslant 42$ region, one can obtain $\gamma_\alpha^2/\gamma_\alpha^2(^{94}\text{Mo})$ for the neighboring nuclei ^{96}Ru and ^{98}Pd through Ref. [12], which analyzed these two nuclei in terms of the α + core structure with the nuclear potential of W.S. + W.S.^{3} shape; taking the values of $\gamma_\alpha^2(^{94}\text{Mo}; 0^+)$, $\gamma_\alpha^2(^{96}\text{Ru}; 0^+)$, and $\gamma_\alpha^2(^{98}\text{Pd}; 0^+)$ from Ref. [12], one obtains $\gamma_\alpha^2/\gamma_\alpha^2(^{94}\text{Mo}) = 0.841$ and 0.702 for ^{96}Ru and ^{98}Pd, respectively. Therefore, the results for ^{96}Ru and ^{98}Pd in Ref. [12] reinforce the indication that there are nuclei around ^{94}Mo with a significant α-clustering degree.

The ^{72}Kr and ^{78}Sr nuclei were analyzed with the band numbers $G_{\text{g.s.}} = 12$ and 14, obtaining higher reduced α-widths with $G_{\text{g.s.}} = 14$. As $G_{\text{g.s.}} = 14$ is more suitable for describing the g.s. bands and rms charge radii (see discussion in the next paragraph), the analysis of the reduced α-widths of ^{72}Kr and ^{78}Sr is focused on the use of $G_{\text{g.s.}} = 14$. In the case of ^{78}Sr, the ratios $\gamma_\alpha^2/\gamma_\alpha^2(^{60}\text{Zn}) = 0.394$ and $\gamma_\alpha^2/\gamma_\alpha^2(^{94}\text{Mo}) = 0.279$ indicate a reasonable α-clustering degree in the 0^+ ground state compared to ^{60}Zn and ^{94}Mo. However, in the case of ^{72}Kr, the ratios $\gamma_\alpha^2/\gamma_\alpha^2(^{60}\text{Zn}) = 1.305$ and $\gamma_\alpha^2/\gamma_\alpha^2(^{94}\text{Mo}) = 0.923$ indicate a relatively high α-clustering degree in the 0^+ ground state, even higher than ^{60}Zn. In addition to its favorable Q_α/A_T position among the Kr isotopes (see Fig. 1), Fig. 6 shows that ^{72}Kr is the nucleus with the highest Q_α/A_T value among the $A = 72$ even-even isobars and the second highest Q_α/A_T value among the $N = 36$ even-even isotones; such features point to ^{72}Kr as one of the preferential nuclei for α clustering in its mass subregion. The relatively high value of $\gamma_\alpha^2(^{72}\text{Kr}; 0^+)$ and the favorable Q_α/A_T position for ^{72}Kr could be associated with a subshell closure effect due to the presence of $N_{\text{core}} = 34$, or due to the proximity of $N_{\text{core}} = 32$; for the time being, experimental investigations point to the existence of subshell closures at $N = 32$ and $N = 34$ in the calcium region (e.g., [50–52]). Such a suggestion needs to be reinforced by a more focused study of the nuclei neighboring ^{72}Kr. The rough reproduction of the $B(E2)$ experimental values for ^{72}Kr is also an aspect to be considered, as discussed further below.

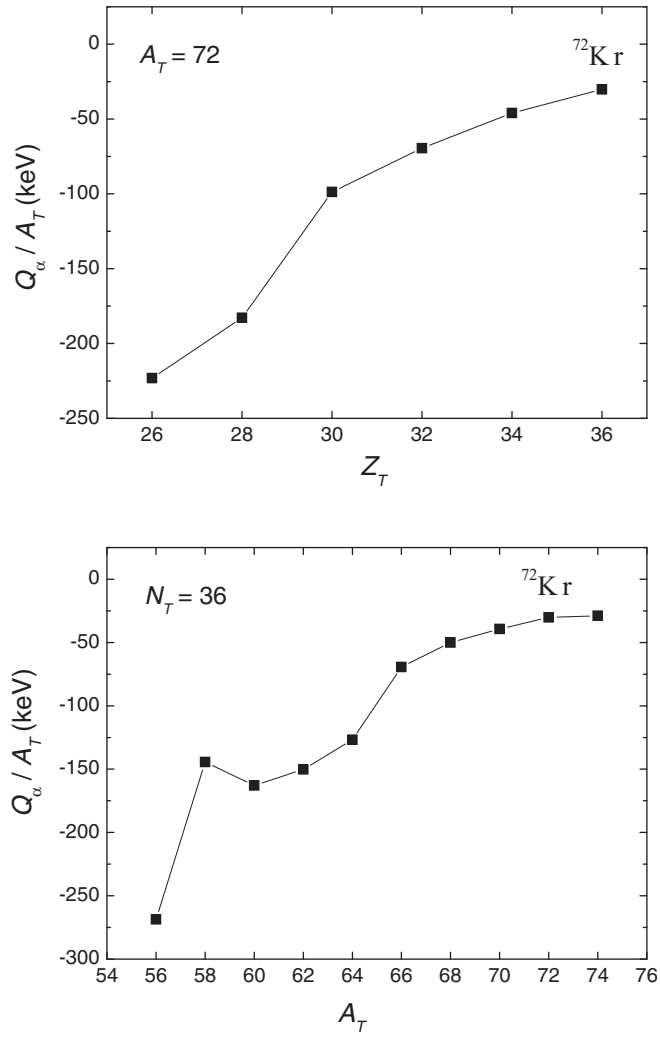

FIG. 6. Q_α/A_T values obtained for the α + core decomposition of even-even $A = 72$ isobars and $N = 36$ isotones. The Q_α/A_T values are shown as a function of the total atomic number Z_T and the total mass number A_T.

The rms charge radius of the total nucleus is given by

$$\langle r^2\rangle_T = \frac{Z_\alpha}{Z_\alpha + Z_{\text{core}}}\langle r^2\rangle_\alpha + \frac{Z_{\text{core}}}{Z_\alpha + Z_{\text{core}}}\langle r^2\rangle_{\text{core}} + \frac{Z_\alpha A_{\text{core}}^2 + Z_{\text{core}} A_\alpha^2}{(Z_\alpha + Z_{\text{core}})(A_\alpha + A_{\text{core}})^2}\langle R^2\rangle, \quad (9)$$

where $\langle r^2\rangle_T^{1/2}$, $\langle r^2\rangle_\alpha^{1/2}$, and $\langle r^2\rangle_{\text{core}}^{1/2}$ are the rms charge radii of the total system, the α cluster, and the core, respectively. The experimental values of $\langle r^2\rangle_\alpha^{1/2}$ and $\langle r^2\rangle_{\text{core}}^{1/2}$ are taken from Ref. [45] and $\langle R^2\rangle^{1/2}$ is assumed to be the calculated rms intercluster separation for the 0^+ ground state. Table IV shows the values obtained for $\langle r^2\rangle_T^{1/2}$ and $\langle r^2\rangle_T^{1/2}/\langle r^2\rangle_{T\,\text{exp}}^{1/2}$. A general evaluation of the results shows there is a good agreement between theoretical and experimental rms radii, since $\langle r^2\rangle_T^{1/2}/\langle r^2\rangle_{T\,\text{exp}}^{1/2}$ is very close to 1 for all the nuclei in

which the calculation was performed. For the ^{72}Kr and ^{78}Sr nuclei, $\langle r^2\rangle_T^{1/2}$ and $\langle r^2\rangle_T^{1/2}/\langle r^2\rangle_{T\,\mathrm{exp}}^{1/2}$ have been calculated in the cases of $G_{\mathrm{g.s.}} = 12$ and 14. It is observed that the use of $G_{\mathrm{g.s.}} = 14$ produces a $\langle r^2\rangle_T^{1/2}/\langle r^2\rangle_{T\,\mathrm{exp}}^{1/2}$ ratio closer to 1 for ^{72}Kr and ^{78}Sr. Therefore, in addition to the results of the spectra, the values of $\langle r^2\rangle_T^{1/2}/\langle r^2\rangle_{T\,\mathrm{exp}}^{1/2}$ indicate that $G_{\mathrm{g.s.}} = 14$ is a more appropriate band number for describing the α + core structure in ^{72}Kr and ^{78}Sr.

In the selected set, one notices there are nuclei with magic N_{core} which have reduced α widths smaller than their respective isotopes without such a feature. This situation occurs for the $N_{\mathrm{core}} = 50$ nuclei ^{84}Ge, ^{86}Se, ^{88}Kr, and ^{90}Sr, which have reduced α widths smaller than ^{64}Ge, ^{68}Se, ^{72}Kr ($G_{\mathrm{g.s.}} = 14$), and ^{78}Sr ($G_{\mathrm{g.s.}} = 14$), respectively. So, it is shown that the magic N_{core} condition does not necessarily determine the isotope with the most pronounced α-cluster structure. The radial wave functions $u(r)$ tend to have smaller amplitude at the nuclear surface for lower Q_α values and in nuclei of greater mass (or greater nuclear radius), contributing to lower values of γ_α^2 in nuclei such as ^{84}Ge, ^{86}Se, ^{88}Kr, and ^{90}Sr. Additionally, γ_α^2 decreases with the increase of the product of the α + core reduced mass and channel radius through the factor $(\hbar^2/2\mu a_c)$. Thus, the isotope with the highest degree of α clustering is defined by the combination of the previously mentioned aspects with the magic/nonmagic core condition.

Another property analyzed is the $B(E2)$ transition rate between the α + core states, given by

$$B(E2; G, J \to J-2) = \frac{15}{8\pi}\,\beta_2^2\,\frac{J(J-1)}{(2J+1)(2J-1)}\left\langle r_{J,J-2}^2\right\rangle^2, \tag{10}$$

where

$$\left\langle r_{J,J-2}^2\right\rangle = \int_0^\infty r^2\, u_{G,J}(r)\, u_{G,J-2}(r)\, dr, \tag{11}$$

β_2 is the recoil factor, given by

$$\beta_2 = \frac{Z_\alpha A_{\mathrm{core}}^2 + Z_{\mathrm{core}} A_\alpha^2}{(A_\alpha + A_{\mathrm{core}})^2}, \tag{12}$$

and $u_{G,J}(r)$ and $u_{G,J-2}(r)$ are the radial wave functions of the initial $|G, J\rangle$ state and final $|G, J-2\rangle$ state, respectively.

The calculated $B(E2)$ values for the $2^+ \to 0^+$ and $4^+ \to 2^+$ transitions, *without* the use of effective charges, are shown in Table V in comparison with experimental data. For some nuclei, $B(E2)$ is calculated only for the $2^+ \to 0^+$ transition when there is not an experimental value available for $4^+ \to 2^+$. When calculating the functions $u_{G,J}(r)$, the depth V_0 was slightly modified to reproduce precisely the corresponding experimental energy levels (see V_0 values in Table V). For comparison, the respective $B(E2)$ values obtained in previous shell-model calculations are shown in Table V (references are indicated in the table). Comparing the calculated and experimental values, it is observed that most of the calculated $B(E2)$ values reproduce the order of magnitude of the respective experimental data. In the cases of ^{52}Ti, ^{58}Ni, ^{90}Sr, and ^{92}Zr, the calculated $B(E2)$ rates are relatively close to the respective experimental values. In general, the results obtained in the shell-model calculations are closer to the experimental $B(E2)$ data; however, it should be taken into account that the shell-model results presented in Table V were obtained with the use of high effective charges in some cases: for protons the effective charge e_π ranges from $1.5\,e$ to $2.32\,e$, and for neutrons the effective charge e_ν ranges from $0.5\,e$ to $1.73\,e$. Therefore, considering that effective charges were not used in the calculations of this work, the $B(E2)$ results obtained by the α + core model are at least satisfactory.

The $B(E2)$ rates for the ^{72}Kr and ^{78}Sr nuclei were calculated in the cases $G_{\mathrm{g.s.}} = 12$ and 14 to make a comparison of the results. The experimental $B(E2)$ rates for ^{72}Kr and ^{78}Sr are significantly higher than in the other selected nuclei. Again, the number $G_{\mathrm{g.s.}} = 14$ is shown to be more suitable for the two nuclei, since this band number produces reasonably higher $B(E2)$ rates; however, the increase in $B(E2)$ produced by $G_{\mathrm{g.s.}} = 14$ is still insufficient for a satisfactory reproduction of the experimental data. If an effective charge δe is applied[1] for the precise reproduction of the experimental $B(E2; 2^+ \to 0^+)$ rate, its value would be $0.674\,e$ for ^{72}Kr ($G_{\mathrm{g.s.}} = 14$) and $1.321\,e$ for ^{78}Sr ($G_{\mathrm{g.s.}} = 14$), meaning a high effective charge for ^{78}Sr. The strong increase in the experimental $B(E2)$ rates and the decrease in the experimental energy spacing $2_1^+ \to 0_1^+$ indicate the increase of collectivity in the transitions in these two nuclei, especially in ^{78}Sr [74]. Therefore, the strong difference between calculated and experimental $B(E2)$ values suggests that the single contribution of the α + core structure in the $2_1^+ \to 0_1^+$ and $4_1^+ \to 2_1^+$ transitions is not sufficient to describe the collective effects manifested in ^{72}Kr and ^{78}Sr.

An analysis of the parameter R is made in relation to $A_T^{1/3}$ and $A_{\mathrm{core}}^{1/3}$. Figure 7 shows the values of R for the set of nuclei analyzed in this work along with ^{20}Ne and ^{212}Po. The R values for ^{20}Ne and ^{212}Po were obtained from our previous work [17] on the same α + core potential applied to nuclei with α clustering above double shell closures. The full squares correspond to the set {^{20}Ne, ^{44}Ti, ^{94}Mo, ^{212}Po} and the open circles correspond to the nuclei from ^{46}Cr to ^{92}Zr selected in this work. Due to the more favorable results for ^{72}Kr and ^{78}Sr by using $G_{\mathrm{g.s.}} = 14$, only the R values related to $G_{\mathrm{g.s.}} = 14$ are shown graphically for these two nuclei. Figure 7 shows the linear trend of the points presented as a function of $A_T^{1/3}$ and $A_{\mathrm{core}}^{1/3}$. An analysis option would be to make a linear fit involving all nuclei, including the set {^{20}Ne, ^{44}Ti, ^{94}Mo, ^{212}Po}; however, such an option would result in a strongly biased fit for the $22 \leqslant Z \leqslant 42$ region, and weakly influenced by the mass regions of ^{20}Ne and ^{212}Po. Therefore, the analysis of the R values was made using the linear fits presented in Ref. [17] for the set {^{20}Ne, ^{44}Ti, ^{94}Mo, ^{212}Po}:

$$R = 1.224\,A_T^{1/3}\ (\mathrm{fm}) \tag{13}$$

and

$$R = 0.694 + 1.092\,A_{\mathrm{core}}^{1/3}\ (\mathrm{fm}). \tag{14}$$

Through Eqs. (13) and (14), it is possible to verify whether the set from ^{46}Cr to ^{92}Zr behaves naturally according to the linear trend previously observed in different mass regions.

[1]The effective charge is defined so that $e_\nu = \delta e$ and $e_\pi = \delta e + e$.

TABLE V. $B(E2)$ rates calculated for the $2_1^+ \to 0_1^+$ and $4_1^+ \to 2_1^+$ transitions in the g.s. bands of the nuclei studied, *without* the use of effective charges. The table shows the depths V_0 fitted to reproduce precisely the experimental energy levels. Experimental data are from Ref. [39], except where indicated. The corresponding $B(E2)$ values obtained from shell-model calculations are shown with the respective references.

Nucleus	J^π	V_0 (MeV)	$B(E2; J \to J-2)$ (W.u.)		
			This work	Expt.	Shell model[a]
^{44}Ti	0^+	220.00			
	2^+	220.22	10.810	22.2(+22 −18) [53]	24.5 [44][c]
	4^+	219.98	14.781	30(+4 −3) [44]	35.4 [44][c]
^{52}Ti	0^+	220.00			
	2^+	220.27	7.909	7.5(+4 −3) [54]	8.7 [55]
	4^+	219.97	10.774	9.4(+14 −11) [54]	11.6 [55]
^{46}Cr	0^+	220.00			
	2^+	220.14	9.657	19(4)	18.7 [56][d]
^{48}Cr	0^+	220.00			
	2^+	220.28	8.858	27(+2 −1) [53]	22.0 [57]
	4^+	219.97	11.950	27(3)	30.1 [57]
^{54}Cr	0^+	220.00			
	2^+	219.98	7.456	14.4(6)	14.8 [55]
	4^+	219.98	10.049	26(9)	19.6 [55]
^{56}Fe	0^+	220.00			
	2^+	220.57	7.106	16.8(7)	12.9 [55]
	4^+	219.96	9.648	24(5)	18.0 [55]
^{58}Fe	0^+	220.00			
	2^+	220.68	6.748	18.5(6)	16.9 [58]
	4^+	220.01	9.168	47(7)	16.7 [58]
^{58}Ni	0^+	220.00			
	2^+	219.09	6.946	9.4(6) [59][b]	3.9 [55]
	4^+	220.00	9.496	3.7(+8 −4) [60]	2.9 [55]
^{60}Ni	0^+	220.00			
	2^+	219.39	6.615	13.0(6) [59][b]	12.9 [61]
	4^+	220.01	9.072	(5.5(17))	5.7 [61]
^{60}Zn	0^+	220.01			
	2^+	220.22	7.252		
^{82}Zn	0^+	220.00			
	2^+	220.10	5.831		
^{64}Ge	0^+	220.00			
	2^+	220.26	6.574	27(4) [62]	26.7 [62]
^{84}Ge	0^+	220.00			
	2^+	220.31	5.790	28(+70 −10) [40]	17.0 [63]
	4^+	220.00	7.926	11(+18 −2) [40]	16.6 [63]
^{68}Se	0^+	220.00			
	2^+	220.21	6.022	24(4) [64]	30.5 [65]
^{86}Se	0^+	220.00			
	2^+	220.41	5.718	20(+5 −2) [40]	19.3 [63]
	4^+	220.05	7.842	$\geqslant$ 5.7	19.5 [63]
^{72}Kr ($G_{\text{g.s.}} = 12$)	0^+	220.02			
	2^+	219.51	5.545	45(8) [66]	1.6 [41], 19.1 [67]
	4^+	220.49	7.363	153(31) [66]	128.5 [41]
^{72}Kr ($G_{\text{g.s.}} = 14$)	0^+	220.00			
	2^+	219.62	8.161	45(8) [66]	1.6 [41], 19.1 [67]
	4^+	220.03	11.060	153(31) [66]	128.5 [41]
^{88}Kr	0^+	220.00			
	2^+	220.33	5.651	12(+10 −4) [40]	14.1 [63]

TABLE V. (*Continued.*)

Nucleus	J^π	V_0 (MeV)	$B(E2; J \to J-2)$ (W.u.) This work	Expt.	Shell model[a]
^{78}Sr ($G_{\text{g.s.}} = 12$)	0^+	220.04			
	2^+	220.66	4.761	93(5) [68]	126 [69]
	4^+	221.74	6.300	169(17)	192 [69]
^{78}Sr ($G_{\text{g.s.}} = 14$)	0^+	220.02			
	2^+	220.31	7.015	93(5) [68]	126 [69]
	4^+	220.86	9.450	169(17)	192 [69]
^{90}Sr	0^+	220.00			
	2^+	220.20	5.565	8.5(+33 −19)	9.7 [70]
	4^+	220.01	7.634	5.2(+11 −7)	5.5 [70]
^{92}Zr	0^+	220.00			
	2^+	219.59	5.619	6.18(23) [71]	6.0 [72]
	4^+	220.02	7.662	4.05(12)	4.4 [72]
^{94}Mo	0^+	220.00			
	2^+	219.90	7.742	16.0(4)	16.5 [73]
	4^+	220.01	10.742	26(4)	17.5 [73]

[a]All shell-model calculations mentioned apply effective charges to protons (e_π) and neutrons (e_ν). For the values shown, e_π ranges from 1.5 e to 2.32 e, and e_ν ranges from 0.5 e to 1.73 e (see specific values in references).
[b]Obtained from the experimental value of $B(E2; 0_1^+ \to 2_1^+)$.
[c]Results obtained with the ZBM2M interaction.
[d]Results obtained with the GXPF1 interaction.

To more accurately assess the linear behavior of R as a function of $A_T^{1/3}$ and $A_{\text{core}}^{1/3}$, Table VI shows the values obtained for the Pearson's correlation coefficient (r_P) for two sets: the first containing the nuclei from ^{46}Cr to ^{92}Zr selected in this work, and the second containing ^{20}Ne, ^{44}Ti, ^{94}Mo, and ^{212}Po. The set from ^{46}Cr to ^{92}Zr has $r_P \approx 0.91$ in relation to $A_T^{1/3}$ and $A_{\text{core}}^{1/3}$, and the set {^{20}Ne, ^{44}Ti, ^{94}Mo, ^{212}Po} has $r_P \approx 0.99$ in relation to the same variables, showing that the linear trend is strong both locally and in nuclei of different mass regions. In the $22 \leqslant Z \leqslant 42$ region, there are two groups of nuclei distanced by ≈0.6 fm on the R scale, corresponding to the quantum numbers $G_{\text{g.s.}} = 12$ and 14, while ^{94}Mo is ≈0.5 fm above the $G_{\text{g.s.}} = 14$ group since it corresponds to $G_{\text{g.s.}} = 16$. Therefore, there is a more abrupt increase in R at the transition from a $G_{\text{g.s.}}$ number to another band number just above, which do not significantly affect the general linear behavior of R.

The standard deviation of the R values related to Eqs. (13) and (14) are calculated for the set {^{20}Ne, ^{44}Ti, ^{94}Mo, ^{212}Po} and the set of nuclei selected from ^{46}Cr to ^{92}Zr (Table VI). In the case of the set {^{20}Ne, ^{44}Ti, ^{94}Mo, ^{212}Po}, S.D. = 0.246 and 0.229 fm in relation to Eqs. (13) and (14), respectively. In the case of the set from ^{46}Cr to ^{92}Zr, S.D. = 0.162 and 0.188 fm in relation to Eqs. (13) and (14), respectively, representing a small relative error for the parameter R which varies from ≈4.6 to ≈5.4 fm in this set. Therefore, the linear relation of R with $A_T^{1/3}$ and $A_{\text{core}}^{1/3}$ is verified both locally ($22 \leqslant Z \leqslant 42$) and in nuclei of different mass regions.

This paragraph discusses the role of the free parameter σ in the (1 + Gaussian)×(W.S. + W.S.^{3}) potential. σ has the function of correctly adjusting the 0^+ ground state at the α + core separation energy (Q_α). It is known that the W.S. + W.S.^{3} nuclear potential provides a satisfactory description in general of the g.s. bands in several nuclei [5,12]; however, the experimental $0^+ \to 2^+$ energy spacing is somewhat roughly described, as it is generally incompatible with the rotational behavior that the W.S. + W.S.^{3} potential produces at the first levels of the band. Figure 8 shows the relation of σ with the 0^+ state energy produced by the W.S. + W.S.^{3} nuclear potential, using the R values from Table I and the

TABLE VI. Pearson's correlation coefficient (r_P) and standard deviation (S.D.) for parameter R in relation to the variables $A_T^{1/3}$ and $A_{\text{core}}^{1/3}$ and the linear fits described in Eqs. (13) and (14). The properties are calculated for the set {^{20}Ne, ^{44}Ti, ^{94}Mo, ^{212}Po} and the set from ^{46}Cr to ^{92}Zr analyzed in this work. The calculations take the R values for ^{72}Kr and ^{78}Sr corresponding to $G_{\text{g.s.}} = 14$.

Set of nuclei	Related variable	Fitted function	r_P	S.D. (fm)
^{46}Cr to ^{92}Zr	$A_{\text{core}}^{1/3}$	Eq. (14)	0.9054	0.188
^{46}Cr to ^{92}Zr	$A_T^{1/3}$	Eq. (13)	0.9062	0.162
^{20}Ne, ^{44}Ti, ^{94}Mo, ^{212}Po	$A_{\text{core}}^{1/3}$	Eq. (14)	0.9932	0.229
^{20}Ne, ^{44}Ti, ^{94}Mo, ^{212}Po	$A_T^{1/3}$	Eq. (13)	0.9912	0.246

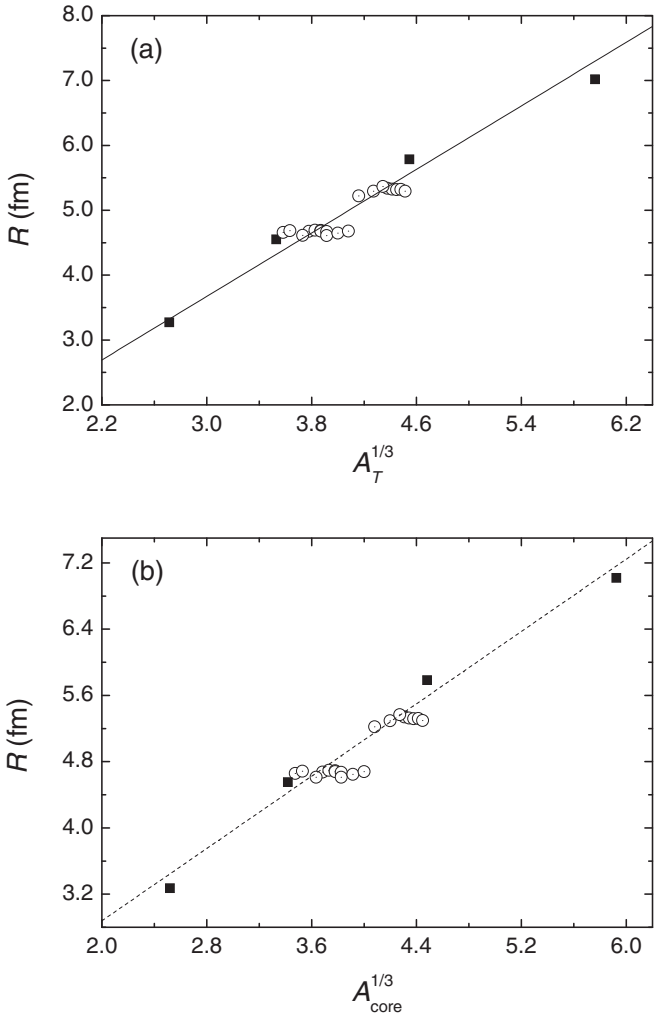

FIG. 7. Values of the parameter R as a function of $A_T^{1/3}$ (a) and $A_{\text{core}}^{1/3}$ (b), where A_T and A_{core} are the mass numbers of the total nucleus and the core, respectively. The full squares correspond to the set {^{20}Ne, ^{44}Ti, ^{94}Mo, ^{212}Po}; the open circles correspond to the set from ^{46}Cr to ^{92}Zr analyzed in this work. The R values shown in the graphs for ^{72}Kr and ^{78}Sr correspond to $G_{\text{g.s.}} = 14$. The full and short dashed lines correspond to the linear fits described by Eqs. (13) and (14), respectively.

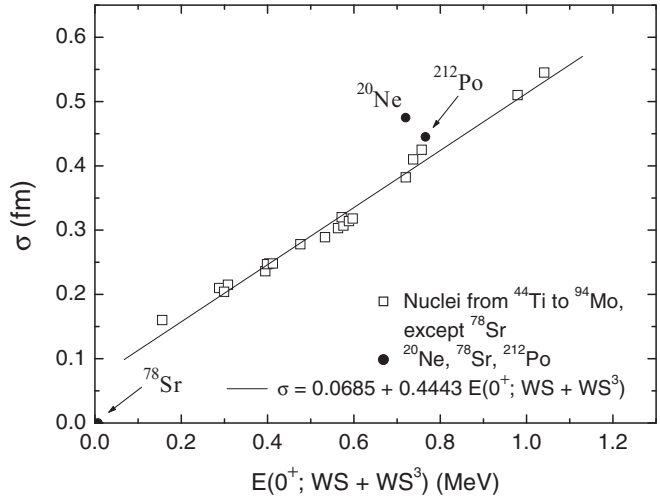

FIG. 8. Values of the parameter σ as a function of the theoretical energy of the 0^+ state produced by the W.S. + W.S.^{3} potential. The σ values presented for ^{72}Kr and ^{78}Sr correspond to $G_{\text{g.s.}} = 14$. The full line shows the linear fit for the nuclei selected from ^{44}Ti to ^{94}Mo, except ^{78}Sr (open squares; see details in the text). The σ values for ^{20}Ne, ^{78}Sr, and ^{212}Po are indicated by full circles.

same fixed parameters a, b, and V_0. In general, the energy $E(0^+;\text{W.S.} + \text{W.S.}^3)$ is above that predicted by the α + core separation (from a few tenths of MeV to ≈1 MeV) since, as in Refs. [5,12], priority is given to more accurate reproduction of the experimental 4^+ level. The σ values of the selected nuclei from ^{44}Ti to ^{94}Mo (except ^{78}Sr) are used for a linear fit as a function of $E(0^+;\text{W.S.} + \text{W.S.}^3)$. The fit shown in Fig. 8 and the corresponding correlation coefficient $r_P = 0.992$ demonstrate the strong linear trend of σ as a function of $E(0^+;\text{W.S.} + \text{W.S.}^3)$ in the $22 \leqslant Z \leqslant 42$ region. The σ value for ^{78}Sr is not included in the fit because it was established beforehand as $\sigma = 0$; in this case, the corresponding experimental spacing $0^+ \to 2^+$ is compatible with a rotational spectrum (see Fig. 4), being suitable to cancel the effect of the (1 + Gaussian) factor for ^{78}Sr.

The σ values for ^{20}Ne and ^{212}Po are shown as full circles in Fig. 8. Note that these two points are slightly distant from the fitted line, mainly ^{20}Ne, indicating that the linear fit of σ as a function of $E(0^+;\text{W.S.} + \text{W.S.}^3)$ should be reevaluated in other mass regions. Despite this, the analysis of the parameter σ clarifies that it becomes greater when the theoretical level $E(0^+;\text{W.S.} + \text{W.S.}^3)$ deviates more strongly from the experimental 0^+ bandhead ($E_x = 0$).

V. DISCUSSION ON THE α + CORE NEGATIVE PARITY BANDS

The (1 + Gaussian)×(W.S. + W.S.^{3}) potential supports excited bands, such as the first negative parity band ($G = G_{\text{g.s.}} + 1$) and the second positive parity band ($G = G_{\text{g.s.}} + 2$). The calculation of the properties of the excited bands involves greater complications compared to the g.s. bands, as many experimental levels at higher energies have undefined spins and parities, or often there are not experimental energy levels corresponding to the calculated levels. The present work focused on the analysis of the g.s. bands; however, the results presented here serve as a starting point for a next study on the excited bands. At this stage, a discussion on the energy location of the negative parity bands is presented for some nuclei of this study in comparison with previous calculations. In the predictions for the negative parity bands below, we use the fixed values of V_0, a, b, and λ (except where other parameter values are explicitly mentioned), and the values of R and σ from Table I.

The existence of a $G = 13$ negative parity band in ^{44}Ti has already been discussed in previous theoretical works (see examples in Refs. [6,8,18,75–77]). The $\alpha + {}^{40}$Ca potential used in this work produces a 1^- bandhead at $E_x = 7.366$ MeV. This value is similar to the previous calculations in

Refs. [6,8,18,75–77], where the 1^- state is in the range of $6 \lessapprox E_x \lessapprox 8$ MeV. The experimental investigation of ^{44}Ti through the ^{40}Ca(^{6}Li, d) ^{44}Ti [26–29] and ^{40}Ca(^{7}Lt, $t\alpha$) ^{40}Ca [31] reactions identified experimental levels from $J^\pi = 1^-$ to 7^- which are candidates for members of the $G = 13$ band, where the experimental level $J^\pi = 1^-$ lies at $E_x = 6.22$ MeV.

In the case of ^{52}Ti, the $\alpha + ^{48}$Ca potential of this work produces $E_x(1^-) = 7.842$ MeV for the $G = 13$ band. This value is above that predicted by Ohkubo [16] [$E_x(1^-) = 6.90$ MeV], which uses a Woods-Saxon squared local potential for the α + core nuclear interaction. The α + core nuclear potential of Ref. [16] was obtained from the real part of an optical potential applied in the analysis of the α-particle scattering from ^{48}Ca, using a depth parameter fitted properly to reproduce the binding energy of the ^{52}Ti ground state. Additional experimental data are needed for the characterization of the $G = 13$ band of ^{52}Ti.

The α + core structure in the ^{46}Cr and ^{54}Cr isotopes was analyzed by the present authors [32] and Mohr [33], with emphasis on the properties of the $G = 12$ g.s. band. Using the α + core potential of the present work, the 1^- bandhead for the $G = 13$ band is obtained at $E_x = 7.806$ MeV for ^{46}Cr and $E_x = 7.902$ MeV for ^{54}Cr. The ^{46}Cr experimental spectrum presents the levels (3^-) ($E_x = 3.196$ MeV), (5^-) ($E_x = 3.987$ MeV), and (7^-) ($E_x = 5.346$ MeV), which can be related to a negative parity band; however, the theoretical prediction $E_x(1^-) = 7.806$ MeV is incompatible with the experimental levels mentioned. In the case of ^{54}Cr, there are no experimental energy levels which can characterize a negative parity band to be compared with theoretical predictions.

In the case of ^{48}Cr, the $\alpha + ^{44}$Ti potential of this work produces $E_x(1^-) = 7.896$ MeV for the $G = 13$ band. In the calculation of Descouvemont on ^{48}Cr [34], which was analyzed in terms of the $\alpha + \alpha + ^{40}$Ca system with the generator coordinate method, the level $J^\pi = 1^-$ of the theoretical $K^\pi = 0^-$ band is predicted at $E_{\rm th} \approx -9.1$ MeV with respect to the $\alpha + \alpha + ^{40}$Ca threshold, i.e., $E_x \approx 3.7$ MeV. In the ^{48}Cr experimental spectrum [39], there are no negative parity levels with defined assignments for an association with the theoretical $E_x(1^-)$ energies mentioned.

A first calculation of ^{64}Ge was presented by Souza *et al.* in Ref. [78] using the (1 + Gaussian)×(W.S. + W.S.^{3}) potential and the same parameters applied in the present work; the $G = 12$ and $G = 13$ bands of the $\alpha + ^{60}$Zn system were calculated, using the depths $V_0 = 220$ MeV and $V_0 = 241$ MeV, respectively. In the case of the $G = 13$ negative parity band, the increase in V_0 was necessary for a better reproduction of the incomplete experimental negative parity band which starts at the $J^\pi = (3^-)$ level with $E_x = 2.970$ MeV. By using $V_0 = 220$ MeV, the 1^- bandhead is found at $E_x = 7.542$ MeV, which is incompatible with the experimental band considered.

In Ref. [12], the present authors showed a study on the α + core structure in ^{90}Sr, ^{92}Zr, ^{94}Mo, ^{96}Ru, and ^{98}Pd nuclei, using a nuclear potential of W.S. + W.S.^{3} shape; in that work, an exploratory calculation of the negative parity bands was made for ^{92}Zr, ^{94}Mo, ^{96}Ru, and ^{98}Pd, where a depth $V_0 = 238$ MeV was employed to give a satisfactory reproduction of the incomplete experimental negative parity bands, while $V_0 = 220$ MeV was applied to the ground state bands. Using the α + core potential of the present work with the fixed depth $V_0 = 220$ MeV, the 1^- bandheads for ^{92}Zr ($G = 15$) and ^{94}Mo ($G = 17$) are found at $E_x = 7.514$ and 7.084 MeV, respectively; the $E_x(1^-)$ value mentioned for ^{94}Mo is similar to other predictions on the $G = 17$ band [7,14,79]. However, the calculated $E_x(1^-)$ values with $V_0 = 220$ MeV are above the experimental bands considered in Ref. [12]. Currently, there are no experimental data for ^{92}Zr and ^{94}Mo that characterize negative parity bands with a bandhead at $E_x \approx 7$ MeV.

New experimental data related to the $22 \leqslant Z \leqslant 42$ region are needed to define whether the depth V_0 is necessarily a band dependent parameter. The calculations presented in Refs. [12,18,78] suggest that the α + core potential should be deeper for a satisfactory description of the negative parity bands of some nuclei in this region. The data obtained through α-transfer reactions are especially important for the characterization of the excited bands in the context of the α + core structure.

VI. SUMMARY AND CONCLUSIONS

This work shows a systematic study of the α + core structure in even-even nuclei of the $22 \leqslant Z \leqslant 42$ region using the local potential model and the nuclear potential of (1 + Gaussian)×(W.S. + W.S.^{3}) shape with two free parameters. This potential has already been successfully tested in nuclei of different mass regions with the same set of fixed parameters [17,32]. A selection criterion based on Q_α/A_T has been applied in the even-Z isotopic chains from Ti to Mo, resulting in 20 selected nuclei of the $22 \leqslant Z \leqslant 42$ region, plus the ^{48}Cr nucleus which was exceptionally included in the comparative study.

The ground state bands of the α + core systems were calculated, producing a good general description of the experimental spectra, mainly from the 0^+ state to the 8^+ state. An important result on the energy spectra is that the model performed similarly both in the nuclei with the α + DCSC configuration and the selected nuclei without such a configuration.

An analysis of the reduced α width, dimensionless reduced α width, and the ratio $\mathcal{R}$ for the 0^+ ground state shows that the ^{44}Ti and ^{94}Mo nuclei have a more pronounced α-cluster structure than other selected nuclei in their respective mass subregions, corroborating the statement that ^{44}Ti and ^{94}Mo are preferential nuclei for α clustering. The ^{60}Zn nucleus has a reduced α width $\gamma_\alpha^2(0^+)$ considerably higher than in other selected nuclei of the same subregion, suggesting this nucleus is also preferential for α clustering. Furthermore, it is indicated there are other nuclei, with or without the α + DCSC configuration, showing a significant α-clustering degree compared to ^{44}Ti, ^{60}Zn, and ^{94}Mo: in the ^{44}Ti subregion, the ^{52}Ti, ^{46}Cr, ^{54}Cr, and ^{48}Cr nuclei stand out with $\gamma_\alpha^2 / \gamma_\alpha^2(^{44}\text{Ti}) = 0.531$, 0.509, 0.278, and 0.254, respectively; in the ^{60}Zn subregion, the ^{56}Fe, ^{58}Fe, ^{58}Ni, ^{60}Ni, ^{64}Ge, and ^{68}Se nuclei stand out with $\gamma_\alpha^2 / \gamma_\alpha^2(^{60}\text{Zn}) = 1.015$, 0.772, 0.810, 0.635, 0.563, and 0.328, respectively; in the ^{94}Mo subregion, the ^{82}Zn and ^{84}Ge nuclei stand out with $\gamma_\alpha^2 / \gamma_\alpha^2(^{94}\text{Mo}) = 0.249$ and 0.278, respectively. A complementary analysis of the results in our

previous work [12] indicates that ^{96}Ru and ^{98}Pd also have an expressive α-clustering degree compared to ^{94}Mo.

The ratio of the calculated rms charge radius for the total nucleus ($\langle r^2\rangle_T^{1/2}$) to the respective experimental rms radius ($\langle r^2\rangle_{T\,\mathrm{exp}}^{1/2}$) was determined for 11 nuclei from the selected set, obtaining ratios above 0.99 in most cases. Very good agreement between calculated and experimental rms radii is demonstrated for the α + core model.

The $B(E2)$ rates were calculated for the $2^+ \to 0^+$ and $4^+ \to 2^+$ transitions of the g.s. band. Most of the calculated values reproduce the order of magnitude of the respective experimental data without the use of effective charges. Concerning the absolute values, there is reasonable agreement between theoretical and experimental $B(E2)$ rates for ^{52}Ti, ^{58}Ni, ^{90}Sr, and ^{92}Zr. Again, it should be noted that the relatively satisfactory results for the $B(E2)$ rates include nuclei with and without the α + DCSC configuration. For ^{72}Kr and ^{78}Sr, it is indicated that the single contribution of the α + core structure in the $2^+ \to 0^+$ and $4^+ \to 2^+$ transitions is not sufficient to describe the strong collectivity observed in the two mentioned nuclei, unless one applies substantial effective charges. Despite the discrepancy between calc. and expt. $B(E2)$ values for ^{72}Kr, the calculated reduced α width $\gamma_\alpha^2(G_{\mathrm{g.s.}} = 14; 0^+)$ suggests this nucleus has a relatively high α-clustering degree in its mass subregion.

It has been observed that the radial parameter R has a clear linear trend with $A_T^{1/3}$ and $A_{\mathrm{core}}^{1/3}$, which has been found locally ($22 \leqslant Z \leqslant 42$) and in nuclei of different mass regions by the set {^{20}Ne, ^{44}Ti, ^{94}Mo, ^{212}Po}. A study of the free parameter σ in the $22 \leqslant Z \leqslant 42$ region indicates a linear trend of σ with the 0^+ state energy predicted by the W.S. + W.S.^{3} nuclear potential.

In conclusion, the local potential model with the (1 + Gaussian)×(W.S. + W.S.^{3}) nuclear potential shows its comprehensiveness in describing the properties of the g.s. bands of $22 \leqslant Z \leqslant 42$ even-even nuclei in terms of an α + core system, providing a good account of the experimental data in general and a systematics applicable even in nuclei without the α + DCSC configuration. In addition to indicating that ^{44}Ti and ^{94}Mo are preferential nuclei for α clustering in their respective mass subregions, the model points the existence of nuclei without the α + DCSC configuration in the $22 \leqslant Z \leqslant 42$ region with a significant α-clustering degree compared to ^{44}Ti, ^{60}Zn, and ^{94}Mo. Applications of the model in other regions, such as $Z < 22$ and $Z > 42$, and the extension of the calculations for the α + core excited bands and odd nuclei are possibilities for future work.

ACKNOWLEDGMENTS

The authors are thankful the HPC resources provided by Information Technology Superintendence (HPC-STI) of University of São Paulo. Support from Instituto Nacional de Ciência e Tecnologia, Física Nuclear e Aplicações (INCT-FNA) is acknowledged.

[1] P. Schuck, in *Proceedings of the 4th International Workshop on "State of the Art in Nuclear Cluster Physics" (SOTANCP4), 13–18 May 2018, Texas*, edited by M. Barbui, C. M. Folden III, V. Z. Goldberg, and G. V. Rogachev, AIP Conf. Proc. No. 2038 (AIP, New York, 2018). p. 020002.
[2] Z. Ren and B. Zhou, Front. Phys. **13**, 132110 (2018).
[3] E. Vardaci, in *Proceedings of the 4th International Workshop on "State of the Art in Nuclear Cluster Physics" (SOTANCP4), 13–18 May 2018, Texas*, edited by M. Barbui, C. M. Folden III, V. Z. Goldberg, and G. V. Rogachev, AIP Conf. Proc. No. 2038 (AIP, New York, 2018). p. 020003.
[4] B. Buck, C. B. Dover, and J. P. Vary, Phys. Rev. C **11**, 1803 (1975).
[5] B. Buck, A. C. Merchant, and S. M. Perez, Phys. Rev. C **51**, 559 (1995).
[6] F. Michel, G. Reidemeister, and S. Ohkubo, Phys. Rev. C **37**, 292 (1988).
[7] S. Ohkubo, Phys. Rev. Lett. **74**, 2176 (1995).
[8] F. Michel, S. Ohkubo, and G. Reidemeister, Prog. Theor. Phys. Suppl. **132**, 7 (1998).
[9] B. Buck, J. C. Johnston, A. C. Merchant, and S. M. Perez, Phys. Rev. C **52**, 1840 (1995).
[10] B. Buck, A. C. Merchant, and S. M. Perez, Phys. Rev. C **61**, 014310 (1999).
[11] F. Michel, G. Reidemeister, and S. Ohkubo, Phys. Rev. C **61**, 041601(R) (2000).
[12] M. A. Souza and H. Miyake, Phys. Rev. C **91**, 034320 (2015).
[13] F. Hoyler, P. Mohr, and G. Staudt, Phys. Rev. C **50**, 2631 (1994).
[14] P. Mohr, Open Nucl. Part. Phys. J. **1**, 1 (2008).
[15] S. M. Wang, J. C. Pei, and F. R. Xu, Phys. Rev. C **87**, 014311 (2013).
[16] S. Ohkubo, Phys. Rev. C **101**, 041301(R) (2020).
[17] M. A. Souza, H. Miyake, T. Borello-Lewin, C. A. da Rocha, and C. Frajuca, Phys. Lett. B **793**, 8 (2019).
[18] T. T. Ibrahim, A. C. Merchant, S. M. Perez, and B. Buck, Phys. Rev. C **99**, 064332 (2019).
[19] D. Bai and Z. Ren, Phys. Rev. C **103**, 044316 (2021).
[20] K. Auranen, D. Seweryniak, M. Albers, A. D. Ayangeakaa, S. Bottoni, M. P. Carpenter, C. J. Chiara, P. Copp, H. M. David, D. T. Doherty, J. Harker, C. R. Hoffman, R. V. F. Janssens, T. L. Khoo, S. A. Kuvin, T. Lauritsen, G. Lotay, A. M. Rogers, J. Sethi, C. Scholey *et al.*, Phys. Rev. Lett. **121**, 182501 (2018).
[21] D. Bai and Z. Ren, Eur. Phys. J. A **54**, 220 (2018).
[22] S. Yang, C. Xu, G. Röpke, P. Schuck, Z. Ren, Y. Funaki, H. Horiuchi, A. Tohsaki, T. Yamada, and B. Zhou, Phys. Rev. C **101**, 024316 (2020).
[23] S. Bailey, T. Kokalova, M. Freer, C. Wheldon, R. Smith, J. Walshe, N. Curtis, N. Soić, L. Prepolec, V. Tokić, F. M. Marqués, L. Achouri, F. Delaunay, Q. Deshayes, M. Parlog, B. Fernández-Dominguez, B. Jacquot, and A. Soylu, Phys. Rev. C **100**, 051302(R) (2019).
[24] S. Bailey, T. Kokalova, M. Freer, C. Wheldon, R. Smith, J. Walshe, N. Soić, L. Prepolec, V. Tokić, F. M. Marqués, L. Achouri, F. Delaunay, M. Parlog, Q. Deshayes, B. Fernández-Dominguez, and B. Jacquot, Eur. Phys. J. A **57**, 108 (2021).
[25] M. Nakao, H. Umehara, R. Nakamoto, S. Ebata, and M. Ito, J. Nucl. Sci. Technol. **57**, 1121 (2020).

[26] T. Yamaya, S. Oh-ami, M. Fujiwara, T. Itahashi, K. Katori, M. Tosaki, S. Kato, S. Hatori, and S. Ohkubo, Phys. Rev. C **42**, 1935 (1990).

[27] P. Guazzoni, M. Jaskola, L. Zetta, C. Y. Kim, T. Udagawa, and G. Bohlen, Nucl. Phys. A **564**, 425 (1993).

[28] T. Yamaya, K. Ishigaki, H. Ishiyama, T. Suehiro, S. Kato, M. Fujiwara, K. Katori, M. H. Tanaka, S. Kubono, V. Guimaraes, and S. Ohkubo, Phys. Rev. C **53**, 131 (1996).

[29] T. Yamaya, K. Katori, M. Fujiwara, S. Kato, and S. Ohkubo, Prog. Theor. Phys. Suppl. **132**, 73 (1998).

[30] H. W. Fulbright, C. L. Bennett, R. A. Lindgren, R. G. Markham, S. C. McGuire, G. C. Morrison, U. Strohbusch, and J. Töke, Nucl. Phys. A **284**, 329 (1977).

[31] M. Fukada, M. K. Takimoto, K. Ogino, and S. Ohkubo, Phys. Rev. C **80**, 064613 (2009).

[32] M. A. Souza and H. Miyake, Eur. Phys. J. A **53**, 146 (2017).

[33] P. Mohr, Eur. Phys. J. A **53**, 209 (2017).

[34] P. Descouvemont, Nucl. Phys. A **709**, 275 (2002).

[35] T. Sakuda and S. Ohkubo, Nucl. Phys. A **712**, 59 (2002).

[36] W. J. Huang, G. Audi, M. Wang, F. G. Kondev, S. Naimi, and X. Xu, Chin. Phys. C **41**, 030002 (2017); M. Wang, G. Audi, F. G. Kondev, W. J. Huang, S. Naimi, and X. Xu, *ibid.* **41**, 030003 (2017).

[37] G. Audi, M. Wang, A. H. Wapstra, F. G. Kondev, M. MacCormick, X. Xu, and B. Pfeiffer, Chin. Phys. C **36**, 1287 (2012); M. Wang, G. Audi, A. H. Wapstra, F. G. Kondev, M. MacCormick, X. Xu, and B. Pfeiffer, *ibid.* **36**, 1603 (2012).

[38] K. Wildermuth and Y. C. Tang, *A Unified Theory of the Nucleus* (Academic Press, New York, 1977).

[39] ENSDF: Evaluated Nuclear Structure Data File, and references therein, `https://www.nndc.bnl.gov/ensdf`

[40] C. Delafosse, D. Verney, P. Marevic, A. Gottardo, C. Michelagnoli, A. Lemasson *et al.*, Phys. Rev. Lett. **121**, 192502 (2018).

[41] K. Kaneko, Y. Sun, and R. Wadsworth, Phys. Scr. **92**, 114008 (2017).

[42] K. Kaneko, T. Mizusaki, Y. Sun, S. Tazaki, and G. de Angelis, Phys. Rev. Lett. **109**, 092504 (2012).

[43] XUNDL: Experimental Unevaluated Nuclear Data List Search and Retrieval, and references therein, https://www.nndc.bnl.gov/xundl

[44] K. Arnswald, P. Reiter, A. Blazhev, T. Braunroth, A. Dewald, M. Droste, C. Fransen, A. Goldkuhle, R. Hetzenegger, R. Hirsch, E. Hoemann, L. Kaya, L. Lewandowski, C. Müller-Gatermann, P. Petkov, D. Rosiak, M. Seidlitz, B. Siebeck, A. Vogt, D. Werner *et al.*, Phys. Rev. C **102**, 054302 (2020).

[45] I. Angeli and K. P. Marinova, At. Data Nucl. Data Tables **99**, 69 (2013).

[46] A. Arima and S. Yoshida, Nucl. Phys. A **219**, 475 (1974).

[47] G. Michaud, L. Scherk, and E. Vogt, Phys. Rev. C **1**, 864 (1970).

[48] T. Li, Y. Luo, and N. Wang, At. Data Nucl. Data Tables **140**, 101440 (2021).

[49] T. Bayram, S. Akkoyun, S. Okan Kara, and A. Sinan, Acta Phys. Pol. B **44**, 1791 (2013).

[50] F. Wienholtz, D. Beck, K. Blaum, Ch. Borgmann, M. Breitenfeldt, R. B. Cakirli, S. George, F. Herfurth, J. D. Holt, M. Kowalska, S. Kreim, D. Lunney, V. Manea, J. Menéndez, D. Neidherr, M. Rosenbusch, L. Schweikhard, A. Schwenk, J. Simonis, J. Stanja, R. N. Wolf *et al.*, Nature (London) **498**, 346 (2013).

[51] D. Steppenbeck, S. Takeuchi, N. Aoi, P. Doornenbal, M. Matsushita, H. Wang, H. Baba, N. Fukuda, S. Go, M. Honma, J. Lee, K. Matsui, S. Michimasa, T. Motobayashi, D. Nishimura, T. Otsuka, H. Sakurai, Y. Shiga, P.-A. Söderström, T. Sumikama *et al.*, Nature (London) **502**, 207 (2013).

[52] E. Leistenschneider, M. P. Reiter, S. AyetSan Andrés, B. Kootte, J. D. Holt, P. Navrátil *et al.*, Phys. Rev. Lett. **120**, 062503 (2018), and references therein.

[53] K. Arnswald, T. Braunroth, M. Seidlitz, L. Coraggio, P. Reiter, B. Birkenbach *et al.*, Phys. Lett. B **772**, 599 (2017).

[54] A. Goldkuhle, C. Fransen, A. Blazhev, M. Beckers, B. Birkenbach, T. Braunroth *et al.* (AGATA Collaboration), Phys. Rev. C **100**, 054317 (2019).

[55] H. Nakada, T. Sebe, and T. Otsuka, Nucl. Phys. A **571**, 467 (1994).

[56] F. A. Majeed, Rom. J. Phys. **53**, 809 (2008).

[57] E. Caurier, A. P. Zuker, A. Poves, and G. Martínez-Pinedo, Phys. Rev. C **50**, 225 (1994).

[58] J. B. McGrory and S. Raman, Phys. Rev. C **20**, 830 (1979).

[59] J. M. Allmond, B. A. Brown, A. E. Stuchbery, A. Galindo-Uribarri, E. Padilla-Rodal, D. C. Radford, J. C. Batchelder, M. E. Howard, J. F. Liang, B. Manning, R. L. Varner, and C.-H. Yu, Phys. Rev. C **90**, 034309 (2014).

[60] C. Loelius, H. Iwasaki, B. A. Brown, M. Honma, V. M. Bader, T. Baugher, D. Bazin, J. S. Berryman, T. Braunroth, C. M. Campbell, A. Dewald, A. Gade, N. Kobayashi, C. Langer, I. Y. Lee, A. Lemasson, E. Lunderberg, C. Morse, F. Recchia, D. Smalley, S. R. Stroberg, R. Wadsworth, C. Walz, D. Weisshaar, A. Westerberg, K. Whitmore, and K. Wimmer, Phys. Rev. C **94**, 024340 (2016).

[61] V. Potbhare, S. K. Sharma, and S. P. Pandya, Phys. Rev. C **24**, 2355 (1981).

[62] K. Starosta, A. Dewald, A. Dunomes, P. Adrich, A. M. Amthor, T. Baumann, D. Bazin, M. Bowen, B. A. Brown, A. Chester, A. Gade, D. Galaviz, T. Glasmacher, T. Ginter, M. Hausmann, M. Horoi, J. Jolie, B. Melon, D. Miller, V. Moeller, R. P. Norris, T. Pissulla, M. Portillo, W. Rother, Y. Shimbara, A. Stolz, C. Vaman, P. Voss, D. Weisshaar, and V. Zelevinsky, Phys. Rev. Lett. **99**, 042503 (2007).

[63] K. Sieja, T. R. Rodríguez, K. Kolos, and D. Verney, Phys. Rev. C **88**, 034327 (2013).

[64] A. J. Nichols, R. Wadsworth, H. Iwasaki, K. Kaneko, A. Lemasson, G. de Angelis *et al.*, Phys. Lett. B **733**, 52 (2014).

[65] K. Kaneko, T. Mizusaki, Y. Sun, and M. Hasegawa, Phys. Lett. B **679**, 214 (2009).

[66] H. Iwasaki, A. Lemasson, C. Morse, A. Dewald, T. Braunroth, V. M. Bader, T. Baugher, D. Bazin, J. S. Berryman, C. M. Campbell, A. Gade, C. Langer, I. Y. Lee, C. Loelius, E. Lunderberg, F. Recchia, D. Smalley, S. R. Stroberg, R. Wadsworth, C. Walz *et al.*, Phys. Rev. Lett. **112**, 142502 (2014).

[67] M. Hasegawa, K. Kaneko, T. Mizusaki, and Y. Sun, Phys. Lett. B **656**, 51 (2007).

[68] R. D. O. Llewellyn, M. A. Bentley, R. Wadsworth, H. Iwasaki, J. Dobaczewski, G. deAngelis, J. Ash, D. Bazin, P. C. Bender, B. Cederwall, B. P. Crider, M. Doncel, R. Elder, B. Elman, A. Gade, M. Grinder, T. Haylett, D. G. Jenkins, I. Y. Lee, B. Longfellow, E. Lunderberg, T. Mijatovic, S. A. Milne, D. Muir, A. Pastore, D. Rhodes, and D. Weisshaar, Phys. Rev. Lett. **124**, 152501 (2020).

[69] K. C. Tripathy and R. Sahu, J. Phys. G: Nucl. Part. Phys. **20**, 911 (1994).

[70] E. A. Stefanova, R. Schwengner, G. Rainovski, K. D. Schilling, A. Wagner, F. Dönau, E. Galindo, A. Jungclaus, K. P. Lieb, O. Thelen, J. Eberth, D. R. Napoli, C. A. Ur, G. de Angelis, M. Axiotis, A. Gadea, N. Marginean, T. Martinez, Th. Kröll, and T. Kutsarova, Phys. Rev. C **63**, 064315 (2001).

[71] A. S. Obeid, O. Burda, M. Chernykh, A. Krugmann, P. von Neumann-Cosel, N. Pietralla, I. Poltoratska, V. Yu. Ponomarev, and C. Walz, Phys. Rev. C **87**, 014337 (2013).

[72] V. Werner, D. Belic, P. von Brentano, C. Fransen, A. Gade, H. von Garrel, J. Jolie, U. Kneissl, C. Kohstall, A. Linnemann, A. F. Lisetskiy, N. Pietralla, H. H. Pitz, M. Scheck, K.-H. Speidel, F. Stedile, and S. W. Yates, Phys. Lett. B **550**, 140 (2002).

[73] A. F. Lisetskiy, N. Pietralla, C. Fransen, R. V. Jolos, and P. von Brentano, Nucl. Phys. A **677**, 100 (2000).

[74] S. L. Rice, Y. Y. Sharon, N. Benczer-Koller, G. J. Kumbartzki, and L. Zamick, Phys. Rev. C **88**, 044334 (2013).

[75] S. Ohkubo, Phys. Rev. C **38**, 2377 (1988).

[76] A. C. Merchant, K. F. Pál, and P. E. Hodgson, J. Phys. G: Nucl. Part. Phys. **15**, 601 (1989).

[77] F. Koyuncu, A. Soylu, and O. Bayrak, Mod. Phys. Lett. A **32**, 1750050 (2017).

[78] M. A. Souza, H. Miyake, T. Borello-Lewin, C. A. da Rocha, and C. Frajuca, J. Phys.: Conf. Ser. **1291**, 012037 (2019).

[79] M. A. Souza and H. Miyake, Braz. J. Phys. **35**, 826 (2005).